HHS Public Access

Author manuscript

Biochim Biophys Acta Mol Cell Res. Author manuscript; available in PMC 2020 December 01.

Published in final edited form as:

Biochim Biophys Acta Mol Cell Res. 2019 December ; 1866(12): 118552. doi:10.1016/j.bbamcr.2019.118552.

LDL receptor related protein 1 requires the I_3 domain of Discs-large homolog 1/DLG1 for interaction with the kinesin motor protein KIF13B

Joslyn Mills[a,1], **Toshihiko Hanada**[b,1], **Yoichi Hase**[b], **Laura Liscum**[a,c], **Athar H. Chishti**[a,b]

[a]Graduate Program in Cellular and Molecular Physiology, Sackler School of Graduate Biomedical Sciences, Tufts University School of Medicine, Boston, MA, USA

[b]Department of Developmental, Molecular and Chemical Biology, Tufts University School of Medicine, Boston MA, USA

[c]Department of Immunology, Tufts University School of Medicine, Boston MA, USA

Abstract

KIF13B, a kinesin-3 family motor, was originally identified as GAKIN due to its biochemical interaction with human homolog of *Drosophila* discs-large tumor suppressor (hDLG1). Unlike its homolog KIF13A, KIF13B contains a carboxyl-terminal CAP-Gly domain. To investigate the function of the CAP-Gly domain, we developed a mouse model that expresses a truncated form of KIF13B protein lacking its CAP-Gly domain (KIF13BΔCG), whereas a second mouse model lacks the full-length KIF13A. Here we show that the KIF13BΔCG mice exhibit relatively higher serum cholesterol consistent with the reduced uptake of [^{3}H]CO-LDL in KIF13BΔCG mouse embryo fibroblasts. The plasma level of factor VIII was not significantly elevated in the KIF13BΔCG mice, suggesting that the CAP-Gly domain region of KIF13B selectively regulates LRP1-mediated lipoprotein endocytosis. No elevation of either serum cholesterol or plasma factor VIII was observed in the full length KIF13A null mouse model. The deletion of the CAP-Gly domain region caused subcellular mislocalization of truncated KIF13B concomitant with the mislocalization of LRP1. Mechanistically, the cytoplasmic domain of LRP1 interacts specifically with the alternatively spliced I_3 domain of DLG1, which complexes with KIF13B via their GUK-MBS domains, respectively. Importantly, double mutant mice generated by crossing KIF13A null and KIF13BΔCG mice suffer from perinatal lethality showing potential craniofacial defects. Together, this study provides first evidence that the carboxyl-terminal region of KIF13B

Corresponding author: A. Chishti, Department of Developmental, Molecular & Chemical Biology, Tufts University School of Medicine, 150 Harrison Avenue, Room 714, Boston, MA. 02111, Tel: (617) 636-3457; Fax: (617) 636-3568; athar.chishti@tufts.edu.

[1]Both authors (JM and TH) contributed equally to this work and should be considered joint first author

Author contributions

J.M. and T.H. designed and performed most of the experiments; Y.H. performed initial characterization of KIF13B mutant mice; J.M. and L.L. designed lipid-based studies; A.C., J.M., and T.H. designed protein binding studies; A.C., J.M., T.H., L.L. contributed in the writing of the manuscript. A.C. is the principal investigator of this study.

Conflict-of-interest disclosure

The authors declare no competing financial interests.

containing the CAP-Gly domain is important for the LRP1-DLG1-KIF13B complex formation with implications in the regulation of metabolism, cell polarity, and development.

Keywords

KIF13B; GAKIN; KIF13A; kinesin; molecular motor; LRP1; DLG1; cholesterol; endocytosis; protein-protein interaction

1. Introduction

The kinesin superfamily of proteins, termed KIFs, are motor proteins that generally transport various cargos towards the plus end of microtubules via anterograde transport. We first identified full length GAKIN (Guanylate Kinase Associated Kinesin) due to its direct binding to the guanylate kinase-like (GUK) domain of human homolog of *Drosophila* discs-large tumor suppressor (hDLG1) [1]. Subsequent bioinformatics analysis identified a homolog of KIF13B that was designated as KIF13A, and this finding led to the re-assignment of GAKIN as KIF13B to be consistent with the kinesin family nomenclature [2]. The KIF13B protein consists of multiple domains including the N-terminal motor domain, followed by the forkhead-associated (FHA) domain, and the MAGUK (membrane-associated GUK) Binding Stalk (MBS) domain. The motor activity of KIF13B is required for the transport of PIP_3-containing vesicles to regulate neuronal cell polarity [3]. The FHA domain of KIF13B directly interacts with centaurin-α_1 (also called PIP_3BP), which in turn activates ADP-ribosylation factor (ARF6) by suppressing the GAP activity of centaurin-α_1 [4]. The MBS domain of KIF13B directly binds to the GUK domain of MAGUKs, such as hDLG1, and permits KIF13B mediated transport of MAGUK-containing vesicles on microtubules [5]. The structure of the GUK domain of DLGTs homolog, DLG4 (also known as PSD-95 or SAP-90), in complex with the MBS domain of KIF13B revealed that their binding mechanism is phosphorylation-independent, and that one key residue, R786, in the MBS domain of KIF13B is crucial for the binding of DLG4 specifically to KIF13B instead of the highly homologous KIF13A [6]. Direct binding of hDLG1 to the MBS domain of KIF13B activates the microtubule-stimulated ATPase activity of KIF13B, suggesting a regulatory role of this domain [7]. Mammalian KIF13B shows homology to the *Drosophila* kinesin-73 motor protein (Khc-73), which recognizes the GUK domain of fly DLG1 for its biochemical and functional interactions [8, 9]. Similarly, KLP4, a motor protein found in *C. elegans,* shows sequence homology to both KIF13B and KIF13A and plays a functional role in glutamate receptor trafficking [10]. Many cellular processes, including the trafficking of VEGFR2 to the plasma membrane to regulate angiogenesis [11], binding to Disheveled to synergistically induce planar cell polarity [12], sorting and trafficking of retrograde BMP signaling in motor neurons [13], regulating PNS and CNS myelination [14], and cilia-dependent Sonic hedgehog signaling [15] have been shown to be dependent on functional KIF13B.

The domain that distinguishes KIF13B from its homolog KIF13A is the Cytoskeleton-Associated Protein Glycine-rich (CAP-Gly) domain located at the C-terminus of KIF13B. Compared to other domains, relatively little is known about the function of the CAP-Gly

domain in KIF13B. In other proteins, such as CLIP170 and Dynactin, the CAP-Gly domain plays a microtubular-based function due to its direct binding to microtubules [16]. Previously, we have shown the microtubule-binding activity of CAP-Gly domain of KIF13B and utilized recombinant CAP-Gly domain of KIF13B to immobilize the microtubules for vesicle motility studies [3]. Another study reported that the CAP-Gly domain of *Drosophila* Khc-73 plays a functional role in microtubule-induced cortical polarity of neuroblasts [8]. Together, the evidence suggests that the CAP-Gly domain of KIF13B stabilizes the motor protein by binding to a parallel microtubule or guiding its cargo to a specific destination in the cell.

A subsequent study has shown that KIF13B plays a functional role in the uptake of lipoproteins through an LDL receptor related protein 1 (LRP1)-dependent mechanism via the FHA-MBS-Coiled coil domains of KIF13B [17]. Using a full length KIF13B knock out mouse model (KIF13B FLKO), it was shown that KIF13B can recruit LRP1 to caveolae by engaging hDLG1 as an adaptor. The functionality of the KIF13B-hDLG1-LRP1 complex was further reinforced by the recruitment of utrophin and centaurin-α_1 via the CC and FHA domains, respectively, to induce LRP1 endocytosis. Guided by our previous findings demonstrating direct binding of the FHA domain of KIF13B to the GAP domain of centaurin-α_1 [4], Hirokawa and colleagues proposed a model rationalizing the enhancement of LRP1 endocytosis and its ligands. The KIF13B FLKO mouse model showed a modest increase of serum cholesterol and factor VIII, likely due to the reduced uptake of LRP1-bound ligands [17]. However, the reported model did not explain how the LRP1 binds to hDLG1, and if the CAP-Gly domain of KIF13B plays any functional role in the endocytosis of LRP1 specific ligands.

Here we report the development of two mouse models: a mouse model expressing a truncated form of KIF13B lacking its C-terminus, which includes the CAP-Gly domain (KIF13BΔCG), and a full-length KIF13A null (KIF13A FLKO) mouse model (Fig. 1). These mouse models allowed us to interrogate the role of the CAP-Gly domain region of KIF13B and assess any compensatory role of KIF13A. We also investigated the biochemical basis of the LRP1-hDLG1 interaction due to its importance in the regulation of LRP1-mediated endocytosis [17]. The hDLG1 protein belongs to a subfamily of MAGUKs that contain multiple PDZ domains, an SH3 domain, and a GUK domain [18]. Moreover, hDLG1 contains an N-terminal L27 domain and several alternatively spliced variants such as insert 2 (I_2) or insert 3 (I_3) located between its SH3 and GUK domains [19]. The I_3 insert, comprised of 34 amino acids, retains the sole binding site for the FERM domain containing protein 4.1 [20], and is required for the membrane targeting of hDLG1 [20]. Importantly, a region termed the HOOK domain located between the SH3 and GUK domains of *Drosophila* DLG, which is similar to the I_3 sequence in hDLG1, is essential for the membrane localization as well as polarity and overgrowth regulation in *Drosophila* DLG [21].

LRP1, a member of the LDL receptor (LDLr) family, is composed of 2 subunits; the large extracellular α subunit and the smaller transmembrane β subunit [22]. LRP1 is more complex as compared to LDLr; its multiple ligand binding repeats located within the a subunit enable it to recognize nearly 40 different ligands. In addition, LRP1 regulates multiple signaling pathways in part due to the cytoplasmic tail (CT) of its β subunit

interacting with several adaptor proteins [23], including endocytosis and PDGF signaling pathways [24, 25]. The cytoplasmic tail of LRP1 can also bind indirectly to β-amyloid precursor protein (APP) via the FE65 adaptor [26]. Finally, post-translational modifications within the cytoplasmic tail of LRP1 have been shown to regulate multiple interactions with adaptor proteins, particularly via phosphorylation of the tyrosine residues embedded within the two NPxY motifs of LRP1-CT [27–29].

In this study, we show that the KIF13BΔCG mouse model manifests a modest elevation of serum cholesterol phenotype similar to the KIF13B FLKO mouse [17]. In contrast, the KIF13A FLKO mice did not show any discernible defect in the endocytosis of LRP1 and serum cholesterol. This finding suggests that the CAP-Gly domain region of KIF13B is involved in the uptake of lipoproteins, possibly through an LRP1-mediated mechanism. Furthermore, we show that the cytoplasmic tail of LRP1 interacts specifically with the alternatively spliced I_3 sequence of hDLG1, and this interaction is not regulated by phosphorylation of LRP1 at tyrosine residue 4507. These results suggest a specific function of the CAP-Gly domain region of KIF13B in receptor-mediated endocytosis as well as reveal an unexpected synergistic role with KIF13A in mammalian development.

2. Materials and methods

2.1. Materials

DMEM (11995-065) and FBS (10437-028) were purchased from Gibco (Thermo Fisher Scientific). FuGENE 6 for transfections was from Promega (E2693). LRP1-Herz was obtained from the laboratory of Dr. Joachim Herz [30], [^{3}H] Cholesteryl oleate (NET746) was a gift from Perkin-Elmer. Mouse IgG was from Santa Cruz (sc-2025). Hoechst from Calbiochem (382061). Antibodies: LRP1 mAb (Abcam ab92544), β-Actin mAb (Sigma A5316), PDI mAb (Cell Signaling 3501), LAMP1 pAb (Abcam ab24170), TGN38 with Alexa Fluor 488 conjugate pAb (Novus Bio), TRX mAb (GenScript), GFP, FLAG (Sigma). Anti-hDLG1 mAb 2D11 [31] and anti-KIF13B mAb 4A05 [3]were developed in our laboratory. The rabbit KIF13B N-terminus affinity purified pAb1246 and KIF13B C-terminus rabbit polyclonal antibody were previously described [1, 3]. Secondary antibodies: Goat Anti-Rabbit HRP conjugate (170-5046) and Goat Anti-Mouse IgG HRP conjugate (170-6516) from Bio-Rad, Alexa Goat Anti-Rabbit 568 from Invitrogen (948491), and Biotin-SP AffiniPure Donkey Anti-Rabbit IgG (711-065-152) and Cy3 Streptavidin (016-160-084) from Jackson ImmunoResearch Labs. Normal donkey block (NDB: 10% Normal Donkey Serum, 5% Non-Fat Dry Milk, 4% BSA, 0.1% TritonX-100 in PBS) was a gift from the Schwob lab at Tufts University School of Medicine. ECL Prime Western Blotting Detection Reagent was from GE Healthcare (RPN2232). Chromogenix Coatest SP4 Factor VIII assay was from Diapharma (82409463). Phusion PCR kit was from NEB (M0530S). Glutathione Sepharose beads were from GE Healthcare (17-0756-01). Primers were designed in house and ordered through Tufts University Core Facility. MEFs were isolated from mice as described below. HEK293T and HepG2 cells were obtained from ATCC. HUVEC line was kindly shared by the Jaffe lab at Tufts University School of Medicine. Restriction enzymes and buffers were from NEB. EconoTaq used for genotyping was purchased from Lucigen (F93366).

2.2. Generation of mouse models

ES cell clones with targeted alleles for KIF13A (AF0553) and KIF13B (AF0005) were obtained from the Knockout Mouse Project (KOMP) Repository at the University of California, Davis. Mouse lines were created in Tufts University Transgenic Animal Core Facility. We are grateful to Dr. Janis Lem, Director of the Transgenic Core Facility, for generously providing technical advice and training during the embryonic stem cell culture, electroporation, and colony selection protocols. The protocol and procedures employed were ethically reviewed and approved by Tufts University IACUC/DLAM, and the authors are in compliance with the US National Research Council's Guide for the Care and Use of Laboratory Animals, the US Public Health Service's Policy on Humane Care and Use of Laboratory Animals, and Guide for the Care and Use of Laboratory Animals.

Primers used for genotyping are:

13aF1 (5'-CATGTGGCCCTTGAACTTGCAAAG-3'),

13aR1 (5'-CTTTAGCTCGGGGGCCTTCATGGC-3'),

13aF2 (5'-AGGGAGCAGCTCTCGCAGGCTGAG-3'),

13aGeoR (5'-CCCTGGATATGGCAGTCTCTAC-3'),

13bF1 (5'-AAAGCCTAATGCAAGGCTGGGAG-3'),

13bR1 (5'-AGAGTGAAGGCAGACTAAAGATGG-3'),

13bGeoR (5'-ATGAGGGAGCAGGGCTCG-3').

2.3. Mouse embryo fibroblasts

Mouse embryo fibroblasts (MEFs) were prepared from day 13.5 embryos and maintained in DMEM with 10% FBS. KIF13B and KIF13A mutant mice were backcrossed to almost pure C57BL/6J background. MEFs from KIF13A and KIF13B double knockout (DKO) were prepared from mixed C57BL/6 x 129 genetic background mice.

2.4. Pull-down assays

The GST-tagged hDLG1 constructs [1, 5, 7] were used for pull-down assays. The GST-fusion proteins were expressed in *E. coli* BL21(DE3) and purified using Glutathione-Sepharose (BD). The hDLG1 fusion proteins were immobilized on Glutathione-Sepharose beads as bait and incubated with lysates from HEK293T cells transfected with either LRP1-Herz or LRP1-Y4507F proteins as prey. The LRP1-Herz or LRP1-Y4507F constructs were transfected in HEK293T cells for 24 hours with Promega FuGENE 6 transfection reagent. Lysates were harvested with NP40-containing lysis buffer with multiple phosphatase and protease inhibitors, and sonicated. The BCA method was to determine total protein concentration.

2.5. Epitope mapping of 4A5 monoclonal antibody

Recombinant expression constructs of KIF13B/GAKIN carboxyl terminus (CT) segments were generated by PCR cloning using standard protocols. Primers containing BamHI and EcoRI adapters were used to amplify corresponding regions of human KIF13B/GAKIN. PCR products were cloned into pET32a plasmid vector and recombinant proteins were expressed in BL21 (DE3) strain of *E. coli.* Bacterial cell extracts expressing recombinant proteins were resolved by 12% SDS-PAGE and analyzed by CBB staining and Western blotting using 4A5 monoclonal antibody.

2.6. Co-Immunoprecipitation

For the KIF13B and KIF13A co-IP experiment, FLAG-KIF13B and GFP-KIF13A were transfected in HEK293 cells. FLAG-KIF13B was immunoprecipitated with FLAG mAb conjugated agarose beads (SIGMA) and GFP-KIF13A was detected by anti-GFP Ab. Alternatively, HepG2 cells, an immortalized cell line from human liver carcinoma, were homogenized in the subcellular fractionation buffer (20 mM Tris-HCl, pH 7.4, 10 mM KCl, 2.0 mM $MgCl_2$, 1.0 mM EDTA and protease inhibitors), and nuclei pellet was removed by centrifugation at 720 x g for five minutes. The membrane fraction was collected by further centrifugation at 100,000 x g for one hour and dissolved in the lysis buffer (20 mM Tris-HCl, pH 7.4, 150 mM NaCl, 0.2% Triton X-100, protease inhibitors). Antibodies used for immunoprecipitation (IP) were anti-hDLG1 mAb 2D11 [31], anti-KIF13B mAb 4A5 [3], and normal mouse IgG (Santa Cruz) for LRP1 Co-IP, and anti-LRP1 rabbit pAb, anti-KIF13B rabbit polyclonal antiserum, and the corresponding pre-immune serum for hDLG Co-IP. Protein A/G PLUS-Agarose (Santa Cruz) beads were used to recover the immune-complex, analyzed by SDS-PAGE and Western blotting with an anti-LRP1 rabbit mAb.

2.7. MT binding activity

Human KIF13B CT (AA1626-1826) and human KIF13A CT (AA1558-1762) in pET32a plasmid were used to express TRX- and His-tagged fusion proteins in *E. coli* BL21 (DE3). Porcine brain tubulin was purchased from Cytoskeleton Inc. Microtubules were assembled in the PME buffer (0.1 M PIPES–NaOH, pH 6.8, 1.0 mM $MgCl_2$, 1.0 mM EGTA, 0.1 mM DTT, 1.0 mM GTP) in the presence of 25 μM Taxol at 35 °C. TRX fusion proteins were mixed with polymerized microtubules in PME buffer with 15 μM Taxol at 35°C for two hours. Microtubules were collected by centrifugation using 42.2 Tl rotor, 30,000 x g for 20 min at 20°C. Equal amounts of the supernatant and pellet fractions were analyzed by SDS-PAGE and CBB staining.

2.8. LRP1 Immunofluorescence

MEFs were seeded on coverslips in DMEM containing 10% FBS for 3 days and fixed with 3% PFA/PBS. Cells were permeabilized with 0.3% Triton X-100 and blocked with Normal Donkey Block (NDB) for one hour. Cells were incubated overnight at 4°C in rabbit anti-LRP1 mAb from Abcam diluted 1:5000 in NDB. Cells were then incubated for one hour each in biotinylated donkey anti-rabbit secondary antibody and then Streptavidin anti-donkey Cy3 tertiary antibody. Cells were washed thoroughly with PBS after each incubation, and nuclei were counterstained with Hoechst and mounted with 90% glycerol in

PBS. Cells were visualized at 400X using Zeiss Axio Scope. Control cells with only secondary and tertiary antibodies were used to assess the background staining.

2.9. Tissue histology and immunohistochemistry

Brain and liver tissue from 6-month old WT and KIF13BΔCG mice were harvested and fixed in 10% formalin for three days. Paraffin embedding, and sectioning were performed at the Tufts Medical Center Pathology Core Facility. Paraffin-embedded brain and liver sections were deparaffinized and rehydrated, and antigen retrieval was accomplished using sodium citrate. Autofluorescence was quenched using quenching solution (2.5 mg/ml ammonium chloride in TBS). Tissues were blocked with normal donkey serum block (NDB) and incubated with a rabbit polyclonal antibody against the N-terminus of KIF13B at a dilution of 1:200 [3] overnight at 4°C. Tissues were then incubated for one hour each in biotinylated donkey anti-rabbit secondary antibody and then Streptavidin anti-donkey Cy3 tertiary antibody. For tissues that were double stained with organelle markers TGN38, PDI, or LAMP1, the process was repeated after a second incubation with the biotinylated donkey anti-rabbit secondary antibody, and an hour incubation with the goat anti-rabbit Alexa 488. Tissues were washed thoroughly with PBS after each incubation, and nuclei were counterstained with Floechst and mounted with 90% glycerol in PBS. Slides were imaged at 400X using Zeiss Axio lmager.M2 microscope and AxioCam MRm and MRc using AxioVision version 4.8 software or at 600X using Olympus FV3000 Confocal microscope with the integrated software. The exposure time and sharpness were kept consistent across all images, as well as any size adjustments and contrast and brightness modifications. Control slides with the secondary and tertiary antibodies only were used to assess the background staining. For LacZ activity staining of mouse embryo and MEFs, the embryo or MEFs were fixed in 0.2% glutaraldehyde in the fixation buffer (0.1 M phosphate buffer, pH 7.3, 5 mM EGTA, 2 mM $MgCl_2$), followed by rinsing with detergent solution (0.1 M phosphate buffer, pH 7.3, 2 mM $MgCl_2$, 0.01% sodium deoxycholate, 0.02% NP-40). LacZ activity was visualized by X-gal staining by incubating samples in the staining buffer (0.1M phosphate buffer, pH, 7.3, 2 mM $MgCl_2$, 0.01% sodium deoxycholate, 0.02% NP-40, 5 mM potassium ferricyanide, 5 mM potassium ferrocyanide, 1.0 mg/ml X-gal). For the counter staining of the MEFs, following LacZ activity staining, the MEFs were further fixed in 4% paraformaldehyde. Microtubules were stained with anti-β-Tubulin monoclonal Ab (TUB2.1, Sigma) and signal was detected by HRP conjugated secondary Ab using diaminobenzidine substrate. Nuclei were stained with the Nuclear Fast Red.

2.10. Measurement of serum lipids and plasma Factor VIII

Serum harvested from WT (n=10), KIF13BΔCG (n=11) and KIF13A −/− (n=8) male mice of average age 4 months was analyzed for total cholesterol, HDL, and directly measured LDL by the Jean Mayer USDA Fluman Nutrition Research Center on Aging (HNCRCA) core facility at Tufts University. Serum triglycerides and vLDL were determined in WT (n=5) and KIF13B C-G (n=6) male mice that were fasted for eight hours before terminal bleed to collect serum. To measure factor VIII in plasma, blood was harvested from 6-month old WT (n=5) and KIF13BΔCG (n=6) male mice via terminal bleed from the vena cava in the presence of acid citrate dextrose (1:10 dilution) as an anticoagulant. Plasma was collected within 30 minutes of harvest by centrifugation and used in the factor VIII assays.

For timed clot formation assay, plasma was mixed with clot activating components and a FibroMeter was used to measure the time until a clot was formed as previously described [32, 33]. For the chromogenic assay, the Chromogenix Coatest SP4 Factor VIII kit (Diapharma) was used per manufacturers' instructions.

2.11. LPDS, LDL, and [^{3}H] LDL production

Lipoprotein-deficient serum was prepared by ultracentrifugation of FBS to remove LDL by omitting the thrombin incubation [34]. LDL was isolated from human blood by ultracentrifugation as previously described [34], [^{3}H]CO-LDL was prepared by combining [^{3}H] cholesteryl oleate and human LDL as previously described [35], resulting in a specific activity of 30 dpm/pmol.

2.12. [^{3}H]CO-LDL uptake and hydrolysis

MEFs were seeded in DMEM containing 10% LPDS and cultured for 3 days. Cells were then incubated with 50 μg/ml [^{3}H]CO-LDL for 3, 4.5, 6, and 7.5 hours. Lipids were extracted with hexane:isopropanol (3:2) solvent and dried under air. Each sample was resuspended in chloroform:methanol (2:1) and thin layer chromatography was performed on silica plates in toluene:ethyl acetate (2:1). [^{3}H]-labeled cholesterol and cholesteryl esters were quantified and normalized relative to the amount of protein per well. The uptake was determined as the sum of labeled cholesterol and cholesteryl esters, and the hydrolysis of LDL was determined as the fraction of labeled cholesterol over total labeled uptake. Each experiment was run in triplicates.

2.13. Cloning and site directed mutagenesis

Primers for LRP1-CT containing BamHI or EcoRI restriction sites were used in Phusion High Fidelity PCR to generate the LRP1-beta construct with LPR1-Herz plasmid as the template. The pET32a plasmid was digested with the same enzymes and ligation products were used to transform DH5α bacterial cells. PCR with the pET32a forward and LRP1 reverse primers was used to confirm the correct inclusion in the pET32a backbone. All plasmids were sequenced. Mutagenesis to convert tyrosine-4507 in the CT tail of LRP1 to phenylalanine (phospho-dead mutation) was performed using Phusion High Fidelity PCR with primers containing the targeted mutation. The LPR1-Herz plasmid was used as the template for PCR.

2.14. Statistical analysis

Data are presented as the mean ± standard error of the mean (SEM). Statistical comparisons were made using analysis of variance (ANOVA) and two-tailed unpaired t-tests. A P value < 0.05 was considered statistically significant.

3. Results

3.1. Generation of KIF13A and KIF13B mutant mouse models

KIF13A FLKO and KIF13BΔCG mice were generated by inserting a β-Geo cassette within each of the respective genes. The genotype and protein expression were verified through

PCR and Western blotting (Fig. 1A & 1B). The insertion of the β-Geo cassette in the KIF13A gene leads to complete knockout of the gene (Fig. 1A, top right), leading to no protein expression (Fig. 1A, bottom right). The insertion of the β-Geo cassette in the KIF13B genomic locus leads to a truncation of the gene, and expression of the truncated protein missing the C-terminal amino acids 1521-1843. The C-terminal segment was replaced with the β-Geo cassette. The missing C-terminus includes a proline-rich domain [11] and a CAP-Gly domain that distinguishes KIF13B from KIF13A (Fig. 1B). The expression of truncated KIF13B protein containing the β-Geo cassette was not identifiable by Western blotting but was verified by the LacZ staining of embryos and mouse embryonic fibroblasts (MEFs) (Fig. 1C and Fig. 3C). Both KIF13A FLKO and KIF13BΔCG mice were viable, born at normal Mendelian ratios, and developed to adulthood. To assess the compensatory role of KIF13B and KIF13A, we attempted to generate a double mutant mouse model in C57BL/6J background by crossing KIF13A FLKO and KIF13BΔCG mice. The double mutant mouse model was designated as DKO. Morphological analysis of the embryos at E14.5-E15.5 did not reveal dying/dead embryos. However, we observed high mortality after birth in the DKO mice. Most of the newborn pups were either dead or cannibalized, and therefore no viable pups could be recovered after day one. Occasionally, we found newborn pups dead at day one (Fig. 1D). These pups seem to have their stomachs filled with air without any milk (Fig. 1D white arrow), suggesting that they are unable to suckle milk properly. Interestingly, morphological evaluation of dead pups revealed relatively short nose appearance and potential craniofacial developmental anomalies that could be the underlying cause of their inability to properly suckle (Fig. 1D arrowheads). This unexpected developmental phenotype appears to be similar to the craniofacial anomalies and cleft palate phenotypes that have been observed in the mouse DLG1 mutant mice [36]. However, our initial analysis of two dead pups recovered at day one did not show any discernible evidence of cleft palate. A detailed characterization of the dead newborn DKO pups was not pursued at this stage since the colony of DKO mice was not sustainable.

As independent mutations, both KIF13A FLKO and KIF13BΔCG mice did not show any obvious craniofacial defects, suggesting the existence of a potential compensatory mechanism between the KIF13 family members. We co-transfected epitope-tagged full length KIF13A (GFP) and KIF13B (FLAG) in mammalian cells and demonstrated their co-precipitation *in vitro* (Fig. 1E). This biochemical interaction suggests that either the two kinesin homologs form a heterodimer or interact via their shared cargo and adaptors for full functionality. Furthermore, unlike KIF13B, which has a well conserved CAP-Gly microtubule binding domain in its C-terminus, KIF13A does not contain an obvious CAP-Gly-like motif in the C-terminus. We tested whether the C-terminal region of KIF13A shows any microtubule-binding activity as compared to the C-terminus of KIF13B. The microtubule-pelleting measurements demonstrated that KIF13B C-terminus precipitated with microtubules, whereas KIF13A C-terminus did not (Fig. 1F). Therefore, the microtubule binding activity of the C-terminal region is a unique feature of KIF13B that is not conserved in KIF13A.

3.2. Effect of deletion of CAP-Gly domain region on cholesterol and factor VIII phenotype

A previous study has shown that KIF13B FLKO mice exhibit increased levels of serum cholesterol and factor VIII, which are known ligands of LRP1 [17]. We measured the levels of serum lipids and plasma factor VIII in our KIF13BΔCG mouse model to determine if the CAP-Gly domain region was required for maintaining the homeostasis of LRP1 ligands. Total serum cholesterol, LDL, HDL, vLDL, (Fig. 2A), and triglycerides (not shown) were analyzed from WT, KIF13BΔCG, and KIF13A FLKO mice. The KIF13BΔCG mice showed significantly elevated levels of total cholesterol ($p = 0.033$) and LDL ($p = 0.0051$), and relatively increased HDL ($p = 0.067$) as compared to WT mice. These data were analyzed using the two-tailed unpaired t test (WT versus each mutant individually). The F test to compare variances was not significant for total cholesterol and HDL measurements. However, the F test was significant for the LDL measurements; therefore, the Welch's correction was administered in the two-tailed unpaired t test. In contrast, the KIF13A FLKO mice did not show any measurable difference in the level of these lipids as compared to WT mice.

To further investigate the biochemical basis of the observed cholesterol phenotype, we measured the uptake of [^{3}H]CO-LDL in MEFs derived from WT and KIF13BΔCG embryos. The uptake and hydrolysis of [^{3}H]CO-LDL over time in MEFs indicate that KIF13BΔCG MEFs exhibit significantly reduced uptake of [^{3}H]CO-LDL at the later time points (Fig. 2C). This reduction occurred without any measurable disruption of hydrolysis in the late endosome/lysosome compartment or cholesterol esterification machinery (data not shown). In addition, we measured the plasma factor VIII levels in WT and KIF13BΔCG mice either by the timed clot assay (Fig. 2B) or Chromogenix colorimetric assay (WT average 98.8±27.1 units/ml, 22.4% activity, SD ±6.2, KIF13BΔCG average 103.6±72 units/ml, 23.5% activity, SD ±16.4). We did not find any significant difference in the factor VIII levels between WT and KIF13BΔCG mice using these assays. It is noteworthy that although the difference was not statistically significant, nearly half of the KIF13BΔCG mice showed elevated levels of plasma factor VIII activity. Therefore, we cannot rule out the possibility that the CAP-Gly domain region of KIF13B plays a functional role in the uptake of factor VIII when a larger cohort of age and sex matched KIF13BΔCG mice are analyzed by more sensitive assays in future studies.

3.3. Effect of deletion of CAP-Gly domain region on KIF13B protein localization

The subcellular localization of the KIF13B protein in WT and KIF13BΔCG mice was analyzed in the brain tissue sections by immunofluorescence microscopy (IF) using a polyclonal antibody that recognizes the N-terminus of KIF13B protein, which is preserved in the KIF13BΔCG mice (Fig. 1B). Of note, specificity of the pAb was confirmed by the co-staining experiments (Supplemental Figure S1). The signals from mAb and pAb were identical in WT mouse brain tissue. As shown in Fig. 3A, the punctate staining pattern of the truncated KIF13B lacking the CAP-Gly domain region is strikingly different from the WT protein. In addition, the expression of truncated KIF13B protein appears to be reduced in the KIF13BΔCG mice; there are more puncta in the WT as compared to KIF13BΔCG cells (Fig. 3A, insets). This finding suggests that the deletion of the CAP-Gly domain region causes KIF13B protein to lose functionality likely due to its mislocalization within the cell. The

mislocalization hypothesis is consistent with the similar expression of WT and mutant KIF13B transcripts in the brain tissue as well as MEFs (Supplemental Figure S2). Since KIF13B is also expressed in the liver, we analyzed liver tissue from WT and KIF13BΔCG mice for similar protein localization studies. However, non-specific staining presumably originating from the excessive auto-fluorescence of liver tissue prevented us from visualizing normal and truncated KIF13B under these conditions.

To further investigate the subcellular localization of the WT and truncated KIF13B proteins, the tissue samples were double stained with LAMP1 (lysosomal marker), PDI (endoplasmic reticulum marker), and TGN38 (trans-Golgi network marker). As shown in Fig. 3B and insets, WT KIF13B exhibits colocalization signal with TGN38 as compared to the other markers, whereas relatively reduced colocalization of truncated KIF13B was observed in the KIF13BΔCG, likely due to the mislocalization of the mutant protein. Comparatively, the KIF13BΔCG protein shows colocalization with LAMP1, suggesting the targeting of mutant protein to the lysosomes. Since the panel of organelle markers used in our study is not exhaustive, further studies are required to precisely determine the subcellular localization of KIF13B and KIF13BΔCG proteins preferably in combination with immunogold electron microscopy.

Since the KIF13BΔCG protein appears to lose its functionality due to its mislocalization, we examined whether the mutant protein retains any of the functions of full length KIF13B. The KIF13BΔCG protein showed dynamic localization upon cell migration in the fibroblasts (Fig. 3C), suggesting its functionality as a motor protein. In confluent culture of fibroblasts isolated from mutant KIF13BΔCG day 13.5 embryos, the KIF13B-LacZ fusion protein was observed as intracellular dots (Fig. 3C, top left and bottom left panels). Counterstaining with Nuclear Fast Red was performed to visualize the position of nuclei in the confluent MEFs (Fig. 3C, bottom left panel). This image shows blue signals of LacZ enzyme activity staining as perinuclear dots in the confluent MEFs resembling the microtubule-organizing center (MTOC) (Figure 3C, lower left panel). Interestingly, in the scratch-induced migrating fibroblasts, the blue dots accumulating at the MTOC disappear (Fig. 3C, top and bottom right panels). Counterstaining with anti-β-Tubulin antibody and Nuclear Fast Red showed that the mutant KIF13B signal was detected as blue dots (red arrows) as well as dispersed blue color (yellow arrow) at the leading edge of migrating cells (Fig. 3C, top and bottom right panels). The dynamic movement of the mutant KIF13B protein in migrating fibroblasts is consistent with its function as a plus end-directed microtubule motor. This observation is not surprising since the mutant KIF13B contains N-terminal motor domain as well as protein-protein interaction domains, including FHA and MBS domains, as potential sites for cargo molecules. The deletion of the C-terminus causes destabilization of the KIF13BΔCG protein complex at the membrane-microtubule interface, which is an essential requirement consistent with the published models of KIF13B function in the *Drosophila* and lymphocyte models [8, 37].

3.4. LRP1 status in fibroblasts lacking the CAP-Gly domain region of KIF13B

MEFs from WT, KIF13A FLKO, and KIF13BΔCG mice were examined to visualize LRP1 localization by immunofluorescence microscopy. The LRP1 staining appeared to be diffuse

in the KIF13BΔCG MEFs as compared to WT MEFs where the LRP1 staining is punctate and relatively more intense (Fig. 3D). In contrast, LRP1 staining in the KIF13A FLKO MEFs was similar to the WT MEFs (data not shown). The diffuse staining of LRP1 observed in the KIF13BΔCG MEFs is likely due to either the reduced amount of LRP1 protein present in these cells or less LRP1 contained within the endosomal vesicles thus resulting in higher receptor density on the cell surface. By Western blotting, the steady state protein expression of LRP1 was not altered in MEFs of different genotypes (Fig. 3E). Human umbilical vein endothelial cells (HUVEC), which do not express LRP1, were used as negative control (Fig. 3E). Our attempts to biotinylate surface proteins to compare the surface density of LRP1 in MEFs were not successful presumably due to the large extracellular α subunit of LRP1 masking the extracellular domain of the β subunit. Similarly, we could not perform double staining of LRP1 and KIF13B in the fibroblasts due to the low abundance of endogenous KIF13B in MEFs.

3.5. Localization of 4A5 monoclonal antibody epitope within the C-terminus of human KIF13B/GAKIN

To determine whether our 4A5 monoclonal antibody can recognize the C-terminal mutant of KIF13B, we performed detailed epitope mapping of KIF13B to determine the precise location of 4A5 epitope (Fig. 4). The 4A5 mAb is of IgG1 subclass (kappa) and shows potent and specific reactivity against human, mouse, rat, and donkey KIF13B polypeptides by Western, immunoprecipitation and immunofluorescence applications. The 4A5 mAb was originally made against the CT11 (1414-1826 AA) fusion protein of human KIF13B (Fig. 4A) [3]. Since the mouse mutant KIF13B has truncation at the C-terminus starting from the 1520 AA position corresponding to human KIF13B sequence (Fig. 4A), it is important to know the precise location of 4A5 mAb epitope to determine whether this antibody can be used to detect the truncated form of the mouse KIF13B mutant. The TRX-CT11 fusion protein runs as a 75 kDa band in SDS-PAGE with some degradation products visible by Coomassie Brilliant Blue (CBB) staining (Fig. 4B, lane 1). Western blotting with an anti-TRX mAb detected a series of degradation products ranging from 75 kDa to 25 kDa (Fig. 4B, lane 2). In parallel, Western blotting with 4A5 mAb detected degradation products ranging from 75 kDa to 40 kDa (Fig. 4B, lane 3). Based on the assumption that degradation takes place from the C-terminus of KIF13B, we speculated that the putative epitope of the 4A5 mAb is not located within the ~35 kDa segment from the C-terminus of KIF13B. This speculation placed the 4A5 mAb epitope near the truncation point of the mouse mutant KIF13B at position 1520 AA. A series of recombinant proteins were generated to further map the 4A5 mAb epitope. Human CT11-1 (1414-1520 AA) construct was designed to include the region just outside the deletion site in the mouse mutant KIF13B. Three additional constructs (CT11-2, CT11-3, CT11-4) contained extended C-termini of human KIF13B (Fig. 4C). Western blotting showed that 4A5 mAb did not detect CT11-1 and CT11-2 but detected the CT11-3 and CT11-4 fusion proteins (Fig. 4D). The CT11 construct served as a positive control. These results demonstrate that 4A5 mAb epitope is located within the 1574-1600 AA segment of human KIF13B (Fig. 4E). Therefore, the 4A5 mAb epitope is not included in the mouse mutant KIF13B protein. It is to be noted that Western blotting of native KIF13B is often technically challenging due to its large size (1843 AA, ~250 kDa) (Fig. 1B) and low transfer efficiency to nitrocellulose. Therefore, the TRX-

CT11-4 fusion protein (Fig. 4C) provides an ideal positive control for 4A5 mAb in future studies investigating the function of KIF13B/GAKIN.

3.6. LRP1 interacts with the I_3 domain of hDLG1

Using tagged protein constructs and immunofluorescence microscopy, a recent study has shown that hDLG1 serves as an adaptor between LRP1 and KIF13B at the membrane [17]. However, further biochemical characterization of the ternary complex between LRP1-hDLG1-KIF13B is required since many transmembrane proteins are known to recognize hDLG1 via its PDZ domains [38]. In fact, the previous study implied that this possibility may indeed be the case for LRP1 recognition of hDLG1 based on their co-localization studies using a dominant negative construct of hDLG1 [17]. To investigate the biochemical basis of LRP1-hDLG1 interaction, we employed a series of defined fusion proteins of hDLG1 and pull-down assays (Fig. 5). Since LRP1 is a Type I transmembrane protein with a 100-amino acid cytoplasmic domain, we generated a TRX-tagged LRP1-cytoplasmic domain construct termed TRX-CT. Several hDLG1 constructs, expressed as GST fusion proteins (Fig. 5A), were used to pull-down the recombinant LRP1-CT expressed in bacteria. None of the hDLG1 constructs interacted with recombinant LRP1-CT protein (data not shown). This observation suggested that the lack of direct interaction between hDLG1 constructs and LRP1-CT could be either due to the post-translational modification(s) lacking in the bacterially expressed LRP1-CT protein or the presence of extracellular segment in LRP1-Herz that may stabilize the conformation of its cytoplasmic domain [27].

As an alternative strategy to detect the biochemical interaction between LRP1 and hDLG1, we used a construct that expresses a longer segment of LRP1 in a mammalian expression system. This construct, designated as LRP1-Herz, includes the cytoplasmic tail of LRP1 as well as the transmembrane domain and part of the extracellular domain including the 6 extracellular EGF-like domains of LRP1. The LRP1-Herz construct produced a protein smaller than the full β subunit by ~30 kDa (229 extracellular amino acids in LRP1-Herz versus 457 extracellular amino acids in LRP1β) (Fig. 5B) [30], thus distinguishing this form from endogenous LRP1 by Western blotting. The LRP1-Herz construct was transfected into HEK293T cells and cell lysates prepared after 24-hour post transfection were used as prey. The GST-hDLG1 fusion proteins expressed in bacteria were used as bait in the pull-down assays (Fig. 5 A & C). The hDLG1 constructs containing the alternatively spliced I_3 insertion, but not the I_2 insertion, successfully pulled down the LPR1-Herz protein (Fig. 5C). Further binding studies indicated that an important requirement for the I_3 interaction was the presence of the GUK domain in the hDLG1 constructs to allow biochemical interaction with the LPR1-Herz protein. The GUK domain alone did not bind to LPR1-Herz protein (Fig. 5C). These findings suggest that the GUK domain of hDLG1 confers stability to the relatively smaller 34 amino acid I_3 sequence that would otherwise be exposed and unstructured, and therefore prone to degradation. Consistent with this model, the GST-I_3 construct without the GUK domain did not bind to LRP1-Herz protein under the same conditions (Fig. 5C). Finally, a comparison of the SH3-I_2-GUK and SH3-I_3-GUK constructs of hDLG1 confirmed that the I_3 sequence is essential for binding to the cytoplasmic tail of LRP1.

3.7. Effect of tyrosine phosphorylation of LRP1 on hDLG1 interaction

Phosphorylation of tyrosine residues at Y4507 and Y4473, located within two NPxY motifs of LRP1-CT, has been shown to regulate various interactions of LRP1 with adaptor proteins [27–29]. The phosphorylation of Y4507 precedes and exposes Y4473 for subsequent phosphorylation reactions [27]. To investigate if the hDLG1 interaction with LRP1 is regulated by phosphorylation of Y4507, we replaced the Y4507 in the LRP1-Herz construct with phenylalanine. This construct termed LRP1-Y4507F, which acts as a phospho-dead mutation, retains the aromatic ring with no impact on protein expression. The SH3-I_3-GUK construct of hDLG1 successfully pulled down both LRP1-Herz and LRP1-Y4507F proteins (Fig. 5D) indicating that the lack of tyrosine phosphorylation of LRP1-CT does not affect its interaction with hDLG1 *in vitro.* In fact, upon equal protein loading optimized by Ponceau staining as shown in Fig. 5D, a semi-quantitative assessment of the LRP1-hDLG1 interaction indicates that the Y4507F mutation in LRP1-CT potentiates LRP1-hDLG1 interaction under these conditions. A complementary *in vivo* analysis of LRP1-hDLG1 interaction will be required to assess the biological significance of this observation.

3.8. Existence of endogenous LRP1 and DLG1 complex

To further investigate the physiological relevance of LRP1-DLG1-KIF13B complex, we performed co-immunoprecipitation experiments from HepG2 human liver cell line that expresses LRP1, DLG1, and KIF13B. Endogenous LRP1 was co-precipitated with DLG1 (Fig. 5E, top), and endogenous DLG1 was co-precipitated with KIF13B (Fig. 5E, bottom) from the detergent solubilized membrane fraction using monoclonal antibodies against either DLG1 or KIF13B, respectively. The 2D11 monoclonal antibody, originally developed in our laboratory, recognizes an epitope located within the N-terminus of hDLG1 [31]. However, we did not detect LRP1 in the immunoprecipitates of anti-KIF13B using a monoclonal antibody against KIF13B. The 4A5 monoclonal antibody, developed in our laboratory, recognizes an epitope located within the C-terminus of human KIF13B (Fig. 4E) [3]. This observation likely reflects the transient nature of KIF13B interaction with LRP1-DLG1 complex in liver cells. Since the biochemical interaction between DLG1 and KIF13B is well established [1], it is plausible that LRP1, DLG1, and KIF13B may form a more stable ternary complex only in polarized hepatocytes harvested as primary cells from the liver (Fig. 5E, bottom). Our attempts to detect DLG1 in the immunoprecipitates of LRP1 were not successful, and likely not feasible because the binding of the LRP1 monoclonal antibody may occlude the DLG1 interaction within the short stretch of the LRP1 cytoplasmic tail. In summary, the presence of LRP1 in the immunoprecipitates of DLG1 demonstrates the existence of an endogenous complex between LRP1 and DLG1 in liver cells.

4. Discussion

The CAP-Gly domain is a highly conserved ~80 amino acid motif generally found in proteins targeted to the plus ends of microtubules [16]. The CAP-Gly domains are known to regulate a variety of intracellular processes, including the dynamics of plus-end tracking proteins at the growing end of microtubules, anterograde transport of organelles/vesicles, α-tubulin detyrosination-tyrosination cycle, assembly of intra-protein switches, and tethering of microtubules to the membrane and cytoskeletal compartments [8, 16, 39, 40]. These

diverse biochemical properties of CAP-Gly domains are consistent with their functional role in cell signaling, migration, polarity, chromosome segregation, and tumorigenesis. Similarly, a critical role of CAP-Gly domains in human diseases has been demonstrated by the identification of mutations in $p150^{Glued}$, a subunit of dynactin, resulting in Perry syndrome and distal hereditary motor neuropathy 7B (FIMN7B) [41–43]. Two independent mutations within the N-terminal CAP-Gly domain of $p150^{Glued}$ lead to two distinct pathologies presumably originating from the loss of dynactin binding to microtubules and CLIP-170 [44]. A deletion in the CAP-Gly domain of tubulin-folding cofactor B (TBCE) causes a fatal disorder manifested by hypoparathyroidism, mental retardation, and facial dysmorphism (HRD) [16]. Additional evidence comes from the functional inactivation of CYLD tumor suppressor that leads to benign skin and hair follicle tumors. These mutations affect the C-terminus of CYLD protein containing three CAP-Gly domains. It is believed that the disruption of the third CAP-Gly of CYLD likely plays a crucial role in disease pathology [45]. Despite considerable evidence for their clinical significance, the precise biological function of CAP-Gly domains remains poorly understood. One potential limitation is the absence of mammalian models specifically lacking the CAP-Gly domains.

Mammalian kinesins are grouped into 15 families encompassing 45 motor proteins [46]. The kinesin-3 family includes 8 members including two homologs termed KIF13A and KIF13B. Among the 45 known kinesins, the KIF13B is the only motor that contains a CAP-Gly domain at its C-terminus. This study reports the first characterization of a mouse model expressing a truncated form of KIF13B lacking its CAP-Gly domain region. In addition, we generated a completely null mouse model of KIF13A and demonstrate an unexpected compensatory role of two kinesins in mammalian development. While the characterization of KIF13A and KIF13B mutant mouse models was underway in our laboratory, Kanai and colleagues reported that KIF13B plays a functional role in the endocytosis of LRP1 [17]. Using a full-length KIF13B null mouse model (KIF13B FLKO), they demonstrated ~25% elevation of serum cholesterol and plasma factor VIII, which are known ligands of LRP1 [23]. The observed increase in the plasma factor VIII in KIF13B FLKO mice was heterogenous showing a large variation in 10 animals analyzed in their study [17].

Unlike KIF13B FLKO model, our mouse model only lacks the C-terminus region that includes the CAP-Gly domain. Our findings also show an increase in the serum lipoprotein levels in KIF13BΔCG mice (Fig. 2), a phenotype similar to KIF13B FLKO mice [17]. However, measurements of plasma factor VIII by two independent assays did not show any statistically significant elevation in the KIF13BΔCG mice (Fig. 2B). This finding suggests that either the CAP-Gly domain region of KIF13B differentially regulates the endocytosis of LRP1 ligands or the observed variation in factor VIII levels requires further validation by utilizing a large number of age and sex matched animals. Generally, an LDLr null background is required for identifying the relative contribution of LRP1 in cholesterol homeostasis. Future experiments assessing the LDL uptake in KIF13BΔCG mice and MEFs, without either LDLr or LRP1, may clarify the precise role of the CAP-Gly domain region of KIF13B in the regulation of LRP1 endocytosis.

To further investigate the biochemical basis of lipid homeostasis in mutant mice, we found that the uptake of [^{3}H]CO-LDL is reduced in fibroblasts generated from the KIF13BΔCG as

compared to WT mice (Fig. 2C). This finding suggests a functional role of the CAP-Gly domain region of KIF13B in LRP1-mediated endocytosis of lipoproteins. We also examined the status of KIF13BΔCG protein in brain sections and found that the truncated protein exhibited altered subcellular localization and reduced expression as compared to the WT protein (Fig. 3A). Using double staining with a selected panel of organelle markers, the subcellular localization studies suggest that relatively higher concentration of WT KIF13B is detected within the trans-Golgi network as compared to lysosomes (LAMP1) and the ER (PDI) (Fig. 3B). Reduced colocalization signal of KIF13BΔCG in the brain may be either due to the lower expression of the mutant protein or its aberrant localization. Of note, in contrast to the wild type KIF13B protein, the mutant KIF13BΔCG protein colocalized with LAMP1 indicating that the mutant protein is targeted to lysosomes for degradation presumably due to its recognition as an aberrant protein. Finally, the LacZ staining of KIF13BΔCG MEFs showed that the mutant protein is localized to the microtubule organizing center (MTOC) in confluent cells (Fig. 3C, left). The observed KIF13B localization in Fig. 3C implies the involvement of KIF13B in targeting hDLG1 to the leading edge of migrating cells where a functional role of hDLG1 is well established. However, a precise role of KIF13B-hDLG1 complex in regulating cell migration as well as its regulatory mechanism of activation remain to be investigated. High resolution live imaging and immunogold electron microscopy would be required to determine the precise subcellular compartments of truncated KIF13B protein expressed in the KIF13BΔCG mice. These findings suggest that the CAP-Gly domain region plays a role in the stabilization and appropriate localization of KIF13B. Future studies are required to sort out the possible effects of the β-geo insert in the KIF13B protein on its folding and localization properties.

We found altered subcellular immuno-localization of LRP1 in KIF13BΔCG MEFs as compared to WT mice (Fig. 3D). Since Western blotting did not show any change in the steady state levels of LRP1 in both genotypes (Fig. 3E), altered LRP1 expression is presumably due to the mislocalization of the receptor. The lack of efficient endocytosis of LRP1 ligands could be attributed to the accumulation of surface LRP1 by the deletion of CAP-Gly domain region of KIF13B. The punctate pattern of LRP1 refers to endosomes whereas the diffuse pattern indicates its expression on the cell surface. High-resolution imaging, sub-cellular fractionation, or surface protein biotinylation approaches would be required to determine the precise localization of LRP1 in KIF13BΔCG MEFs harvested from the mutant mice reported in this study.

Since LRP1 does not directly bind to KIF13B, Kanai and colleagues proposed that hDLG1 may function as an adaptor that links LRP1 with KIF13B [17]. In their study, disruption of LRP1 localization in fibroblasts using a dominant negative mutant of hDLG1 implied that LRP1 may bind to the amino terminal half of hDLG1. This model appears to be consistent with the premise that the C-termini of multiple transmembrane proteins recognize the PDZ domains of adaptor proteins [47]. Using pull-down assays, we tested the LRP1-hDLG1 interaction and concluded that the LRP1 cytoplasmic tail does not bind to the three PDZ domains present within the N-terminal half of hDLG1. Further scanning of other hDLG1 domains revealed that LRP1 cytoplasmic tail specifically recognizes the I_3 domain of hDLG1 (Fig. 5C). Our previous studies have shown that the alternatively spliced I_3 motif, flanked by the SH3 and GUK domains in hDLG1, binds to the FERM domain of protein 4.1

family of cytoskeletal proteins [20]. In addition, we have shown that the SFI3-I_3-GUK, but not SH3-I_2-GUK, module of hDLG1 activates the microtubule-stimulated ATPase activity of KIF13B by 10-fold [7]. Genetic studies of *Drosophila* discs large tumor suppressor protein (Dlg) have shown that the HOOK domain, which corresponds to the I_3 motif in hDLG1, is essential for maintaining the epithelial structure and growth regulation [21]. This observation is consistent with our previous findings that the I_3 motif plays a critical role in recruiting hDLG1 to the plasma membrane of epithelial cells [20]. To test if the interaction of LRP1 with hDLG1 is regulated by phosphorylation, we mutated tyrosine-4507 to phenylalanine in LRP1-Herz to mimic a phospho-dead mutation. Our findings show that the LRP1-hDLG1 interaction does not require the phosphorylation at Y4507 on LRP1-Herz. These observations raise the possibility that LRP1 interaction with the I_3 domain of hDLG1 may constitute a novel switch that regulates the cytoskeletal reorganization affecting clustering and localization of receptors by KIF13B. Guided by these findings, we propose a model (Fig. 6) whereby a specific domain of hDLG1 serves as an adaptor by linking LRP1 with KIF13B. The LRP1-CT binds to the I_3 domain of hDLG1, which in turn utilizes its GUK domain to bind to the MBS domain of KIF13B. The truncated KIF13B expressed in KIF13BΔCG mice (Fig. 6B) is mislocalized within the cell, or destabilized at the membrane, thus preventing its interaction with hDLG1 and suppressing LRP1 endocytosis.

We generated KIF13A null mice to assess the compensatory role of a closely related kinesin homolog in LRP1 endocytosis. Unlike KIF13B, KIF13A lacks a CAP-Gly domain and does not bind to either microtubules (Fig. 1F) or hDLG1. The KIF13A null mice did not show any effect on serum cholesterol level (Fig. 2A). A previous study has shown that KIF13A interacts with the clathrin adaptor AP-1 and transports endosomes fused with melanosomes, as well as regulates the formation of endosomal tubules [48, 49]. KIF13A is also known to transport Mannnose-6-Phosphate receptor, and Serotonin Type 1A receptor modulating anxiety [50, 51]. We bred our KIF13A null mice to nearly homogeneous C57BL/6J genetic background but did not observe any coat color defect, which contrasts with the predicted functional role of KIF13A in melanosomes [48, 49]. In the future, our KIF13A null and KIF13BΔCG mutant mice could serve as useful models for testing the role of these kinesins in behavior and anxiety phenotypes.

Our repeated attempts to generate a viable double mutant mouse model of KIF13A and KIF13BΔCG were not successful. Although both KIF13A null and KIF13BΔCG mutant mice are viable and breed normally, the double mutation leads to early perinatal lethality. Occasionally, dead pups recovered from the double mutation breeding show developmental anomalies reminiscent of the developmental defects seen in the mouse models lacking mouse DLG1 and CASK [36, 52, 53]. The cleft palate phenotype previously reported in a DLG1 mutant mouse [36] and a CASK (another MAGUK) mutant mouse [53] led to the death of newborn pups within 24 hours due to defective suckling. Since DLG1 and CASK form a functional complex in epithelia [54], a possibility exists that the perturbation of DLG1-regulated functions manifest in defective craniofacial development. The fact that KIF13B and KIF13A double mutant mouse model showed craniofacial abnormality, similar to DLG1 mutant mouse model, suggests that a functional crosstalk between KIF13A and KIF13B may exist in regulating the DLG1-CASK pathway. It is noteworthy that fully developed dead pups from the double mutant breeding were observed only when the genetic

background of individual KIF13A null and KIF13BΔCG mutant mice was estimated to be ~98% C57BL/6J and ~2% 129/SvJ. Based on these observations, we surmise that the double mutation lacking both full length KIF13A and KIF13B would be lethal in mice with pure C57BL/6J genetic background.

The unexpected mortality observed in the double mutant mice of KIF13A and KIF13BΔCG mice suggests that the two kinesin homologs may function together *in vivo.* This model is consistent with the co-precipitation of two kinesins upon co-transfection of epitope-tagged full length KIF13A and KIF13B in mammalian cells (Fig. 1E). The biochemical interaction between KIF13B and KIF13A suggests that either the two kinesins form a heterodimer or interact via their shared cargo and adaptors for full functionality. Our findings showing a functional inter-dependence of two motors *in vivo* would predict more robust phenotypes in the double mutant cellular models as compared to single knockouts. Another useful feature of our mouse models is the presence of the LacZ protein, which enables direct visualization of KIF13 fusion proteins by X-gal staining. Indeed, the KIF13B-LacZ expression was observed throughout the body with particularly intense expression of KIF13BΔCG along the spinal cord in day 12.5 whole embryos as well as the leading edge of migrating MEFs (Fig. 1C and Fig. 3C). This pattern of KIF13B-LacZ staining is consistent with the endogenous localization of hDLG1 at the leading edge of migrating cells [55, 56]. Our mouse models would be useful for future studies of KIF13A and KIF13B expression and localization of their cargo in a variety of experimental settings.

In summary, our results demonstrate that mutant KIF13B lacking its CAP-Gly domain region retains its motor activity and can translocate to the membrane in transfected mammalian cells, although it may not have a full capacity to transport its cargo. This impairment leads to an overall mislocalization or destabilization of truncated KIF13B, thus preventing the mutant KIF13B from regulating LRP1 endocytosis *in vivo.* Future characterization of these mouse models will enhance the mechanistic understanding of LRP1 endocytosis with implications in hypercholesterolemia and developmental defects.

Supplementary Material

Refer to Web version on PubMed Central for supplementary material.

Acknowledgements

The KIF13 targeting vectors were generated by the trans-NIH Knock-Out Mouse Project (KOMP) at the University of California, Davis. NIH grants to Velocigene at Regeneron Inc. (U01FIG004085) and the CSD Consortium (U01FIG004080) funded the generation of gene-targeted ES cells for 8,500 genes in the KOMP Program and archived and distributed by the KOMP Repository at UC Davis and CHORI (U42RR024244). We are grateful to Dr. Janis Lem of Tufts Transgenic Core Facility for technical help with the generation of KIF13B and KIF13A mutant mouse models, Dr. Lauren Richie of Tufts Division of Laboratory Animal Medicine (DLAM) for assistance with mouse organ microscopy and pathology, Dr. Roderick Bronson at Harvard Medical School for pathological analysis of liver and brain sections, Dr. Yunzhe Lu for technical assistance during the generation of mutant ES cell lines, Bina Julian for optimization of the lacZ staining of mutant mice, and Kaori Yamada for KIF13A and KIF13B immunoprecipitation studies. We are thankful for Madhumouli Chatterjee from Dr. Gary Gilbert's laboratory at the Boston VA Hospital for performing the timed clot assays. We are indebted to Dr. Joachim Herz and Rebekah Hewitt for their gift of the LPR1-Herz construct, Alice Lichtenstein and HNRC Nutrition Evaluation Lab personnel including Gayle Petty and Stephanie Thea Leon Valliere, who performed the lipid profile analysis on mouse blood samples, and Nathan Li from the TUSM histology core for embedding, sectioning, and H&E staining tissues. Finally, we are grateful to Donna-Marie Mironchuk for her invaluable contributions in the administrative and

technical management of the project, development of figures, and proof reading of the manuscript. This work was supported in part by the National Institutes of Health Grants HL060961, HL095050, HL089517, HL051445, Grant-in-Aid from the American Heart Association, and Tufts Collaborates Grant Program.

Abbreviations:

CAP-Gly	Cytoskeleton-Associated Protein Glycine-rich
CG	CAP-Gly
CC	coiled coil
CT	cytoplasmic tail
FHA	forkhead associated
GUK	guanylate kinase-like
GAKIN	guanylate kinase associated kinesin
hDLG1	human discs large tumor suppressor 1
LRP1	LDL-receptor Related Protein 1
LDL	low density lipoprotein
LDLr	low density lipoprotein receptor
LPDS	lipoprotein-deficient serum
MEFs	mouse embryonic fibroblasts
MAGUK	membrane-associate guanylate kinase
MD	motor domain
MTOC	microtubule-organizing center
NC	neck coiled coil

References

[1]. Hanada T, Lin L, Tibaldi EV, Reinherz EL, Chishti AH, GAKIN, a novel kinesin-like protein associates with the human homologue of the Drosophila discs large tumor suppressor in T lymphocytes, J. Biol. Chem, 275 (2000) 28774–28784. [PubMed: 10859302]

[2]. Miki H, Setou M, Kaneshiro K, Hirokawa N, All kinesin superfamily protein, KIF, genes in mouse and human, Proc. Natl. Acad. Sci. U. S. A, 98 (2001) 7004–7011. [PubMed: 11416179]

[3]. Horiguchi K, Hanada T, Fukui Y, Chishti AH, Transport of PIP3 by GAKIN, a kinesin-3 family protein, regulates neuronal cell polarity, J. Cell Biol, 174 (2006) 425–436. [PubMed: 16864656]

[4]. Venkateswarlu K, Hanada T, Chishti AH, Centaurin-alpha1 interacts directly with kinesin motor protein KIF13B, J. Cell Sci, 118 (2005) 2471–2484. [PubMed: 15923660]

[5]. Asaba N, Hanada T, Takeuchi A, Chishti AH, Direct interaction with a kinesin-related motor mediates transport of mammalian discs large tumor suppressor homologue in epithelial cells, J. Biol. Chem, 278 (2003) 8395–8400. [PubMed: 12496241]

[6]. Zhu J, Shang Y, Xia Y, Zhang R, Zhang M, An Atypical MAGUK GK Target Recognition Mode Revealed by the Interaction between DLG and KIF13B, Structure, 24 (2016) 1876–1885. [PubMed: 27642159]

[7]. Yamada KH, Hanada T, Chishti AH, The effector domain of human Dlg tumor suppressor acts as a switch that relieves autoinhibition of kinesin-3 motor GAKIN/KIF13B, Biochemistry (Mosc). 46 (2007) 10039–10045.

[8]. Siegrist SE, Doe CQ, Microtubule-induced Pins/Galphai cortical polarity in Drosophila neuroblasts, Cell, 123 (2005) 1323–1335. [PubMed: 16377571]

[9]. Lu MS, Prehoda KE, A NudE/14-3-3 pathway coordinates dynein and the kinesin Khc73 to position the mitotic spindle, Developmental cell, 26 (2013) 369–380. [PubMed: 23987511]

[10]. Monteiro MI, Ahlawat S, Kowalski JR, Malkin E, Koushika SP, Juo P, The kinesin-3 family motor KLP-4 regulates anterograde trafficking of GLR-1 glutamate receptors in the ventral nerve cord of Caenorhabditis elegans, Mol. Biol. Cell, 23 (2012) 3647–3662. [PubMed: 22855524]

[11]. Yamada KH, Nakajima Y, Geyer M, Wary KK, Ushio-Fukai M, Komarova Y, Malik AB, KIF13B regulates angiogenesis through Golgi to plasma membrane trafficking of VEGFR2, J. Cell Sci, 127 (2014) 4518–4530. [PubMed: 25128562]

[12]. Ossipova O, Chu CW, Fillatre J, Brott BK, Itoh K, Sokol SY, The involvement of PCP proteins in radial cell intercalations during Xenopus embryonic development, Dev. Biol, 408 (2015) 316–327. [PubMed: 26079437]

[13]. Liao EH, Gray L, Tsurudome K, El-Mounzer W, Elazzouzi F, Baim C, Farzin S, Calderon MR, Kauwe G, Haghighi AP, Kinesin Khc-73/KIF13B modulates retrograde BMP signaling by influencing endosomal dynamics at the Drosophila neuromuscular junction, PLoS Genet, 14 (2018) e1007184. [PubMed: 29373576]

[14]. Noseda R, Guerrero-Valero M, Alberizzi V, Previtali SC, Sherman DL, Palmisano M, Huganir RL, Nave KA, Cuenda A, Feltri ML, Brophy PJ, Bolino A, Kif13b Regulates PNS and CNS Myelination through the Dlg1 Scaffold, PLoS Biol, 14 (2016) e1002440. [PubMed: 27070899]

[15]. Schou KB, Mogensen JB, Morthorst SK, Nielsen BS, Aleliunaite A, Serra-Marques A, Furstenberg N, Saunier S, Bizet AA, Veland IR, Akhmanova A, Christensen ST, Pedersen LB, KIF13B establishes a CAV1-enriched microdomain at the ciliary transition zone to promote Sonic hedgehog signalling, Nat Commun, 8 (2017) 14177. [PubMed: 28134340]

[16]. Steinmetz MO, Akhmanova A, Capturing protein tails by CAP-Gly domains, Trends Biochem. Sci, 33 (2008) 535–545. [PubMed: 18835717]

[17]. Kanai Y, Wang D, Hirokawa N, KIF13B enhances the endocytosis of LRP1 by recruiting LRP1 to caveolae, J. Cell Biol, 204 (2014) 395–408. [PubMed: 24469637]

[18]. Zhu J, Shang Y, Chen J, Zhang M, Structure and function of the guanylate kinase-like domain of the MAGUK family scaffold proteins, Frontiers in Biology, 7 (2012) 379–396.

[19]. Lue RA, Marfatia SM, Branton D, Chishti AH, Cloning and characterization of hdlg: the human homologue of the Drosophila discs large tumor suppressor binds to protein 4.1, Proc. Natl. Acad. Sci. U. S. A, 91 (1994) 9818–9822. [PubMed: 7937897]

[20]. Hanada T, Takeuchi A, Sondarva G, Chishti AH, Protein 4.1-mediated membrane targeting of human discs large in epithelial cells, J. Biol. Chem, 278 (2003) 34445–34450. [PubMed: 12807908]

[21]. Hough CD, Woods DF, Park S, Bryant PJ, Organizing a functional junctional complex requires specific domains of the Drosophila MAGUK Discs large, Genes Dev, 11 (1997) 3242–3253. [PubMed: 9389655]

[22]. Herz J, Kowal RC, Ho YK, Brown MS, Goldstein JL, Low density lipoprotein receptor-related protein mediates endocytosis of monoclonal antibodies in cultured cells and rabbit liver, J. Biol. Chem, 265 (1990) 21355–21362. [PubMed: 2250029]

[23]. Lillis AP, Van Duyn LB, Murphy-Ullrich JE, Strickland DK, LDL receptor-related protein 1: unique tissue-specific functions revealed by selective gene knockout studies, Physiol. Rev, 88 (2008) 887–918. [PubMed: 18626063]

[24]. Craig J, Mikhailenko I, Noyes N, Migliorini M, Strickland DK, The LDL receptor-related protein 1 (LRP1) regulates the PDGF signaling pathway by binding the protein phosphatase SHP-2 and

modulating SHP-2-mediated PDGF signaling events, PLoS One, 8 (2013) e70432. [PubMed: 23922991]

[25]. Lillis AP, Mikhailenko I, Strickland DK, Beyond endocytosis: LRP function in cell migration, proliferation and vascular permeability, Journal of Thrombosis and Haemostasis, 3 (2005) 1884–1893. [PubMed: 16102056]

[26]. Pietrzik CU, Yoon I-S, Jaeger S, Busse T, Weggen S, Koo EH, FE65 Constitutes the Functional Link between the Low-Density Lipoprotein Receptor-Related Protein and the Amyloid Precursor Protein, The Journal of Neuroscience, 24 (2004) 4259–4265. [PubMed: 15115822]

[27]. Betts GN, van der Geer P, Komives EA, Structural and functional consequences of tyrosine phosphorylation in the LRP1 cytoplasmic domain, J. Biol. Chem, 283 (2008) 15656–15664. [PubMed: 18381291]

[28]. Klug W, Dietl A, Simon B, Sinning I, Wild K, Phosphorylation of LRP1 regulates the interaction with Fe65, FEBS Lett, 585 (2011) 3229–3235. [PubMed: 21968187]

[29]. Guttman M, Betts GN, Barnes H, Ghassemian M, van der Geer P, Komives EA, Interactions of the NPXY microdomains of the low density lipoprotein receptor-related protein 1, Proteomics, 9 (2009) 5016–5028. [PubMed: 19771558]

[30]. Herz J, Hamann U, Rogne S, Myklebost O, Gausepohl H, Stanley KK, Surface location and high affinity for calcium of a 500-kd liver membrane protein closely related to the LDL-receptor suggest a physiological role as lipoprotein receptor, EMBO J, 7 (1988) 4119–4127. [PubMed: 3266596]

[31]. Lin H-T, Steller MA, Aish L, Hanada T, Chishti AH, Differential expression of human Dlg in cervical intraepithelial neoplasias, Gynecol. Oncol, 93 (2004) 422–428. [PubMed: 15099956]

[32]. Shi J, Gilbert GE, Lactadherin inhibits enzyme complexes of blood coagulation by competing for phospholipid-binding sites, Blood, 101 (2003) 2628–2636. [PubMed: 12517809]

[33]. Gilbert GE, Novakovic VA, Shi J, Rasmussen J, Pipe SW, Platelet binding sites for factor VIII in relation to fibrin and phosphatidylserine, Blood, 126 (2015) 1237–1244. [PubMed: 26162408]

[34]. Goldstein JL, Basu SK, Brown MS, Receptor-mediated endocytosis of low-density lipoprotein in cultured cells, Methods Enzymol, Academic Press, Place Published, 1983, pp. 241–260.

[35]. Faust JR, Goldstein JL, Brown MS, Receptor-mediated uptake of low density lipoprotein and utilization of its cholesterol for steroid synthesis in cultured mouse adrenal cells, J. Biol. Chem, 252 (1977) 4861–4871. [PubMed: 194897]

[36]. Caruana G, Bernstein A, Craniofacial dysmorphogenesis including cleft palate in mice with an insertional mutation in the discs large gene, Mol. Cell. Biol, 21 (2001) 1475–1483. [PubMed: 11238884]

[37]. Lamason RL, Kupfer A, Pomerantz JL, The dynamic distribution of CARD11 at the immunological synapse is regulated by the inhibitory kinesin GAKIN, Mol. Cell, 40 (2010) 798–809. [PubMed: 21145487]

[38]. Fanning AS, Anderson JM, Protein–protein interactions: PDZ domain networks, Curr. Biol, 6 (1996) 1385–1388. [PubMed: 8939589]

[39]. Gao J, Huo L, Sun X, Liu M, Li D, Dong JT, Zhou J, The tumor suppressor CYLD regulates microtubule dynamics and plays a role in cell migration, J. Biol. Chem, 283 (2008) 8802–8809. [PubMed: 18222923]

[40]. Wickstrom SA, Masoumi KC, Khochbin S, Fassler R, Massoumi R, CYLD negatively regulates cell-cycle progression by inactivating HDAC6 and increasing the levels of acetylated tubulin, EMBO J, 29 (2010) 131–144. [PubMed: 19893491]

[41]. Farrer MJ, Hulihan MM, Kachergus JM, Dachsel JC, Stoessl AJ, Grantier LL, Calne S, Calne DB, Lechevalier B, Chapon F, Tsuboi Y, Yamada T, Gutmann L, Elibol B, Bhatia KP, Wider C, Vilarino-Guell C, Ross OA, Brown LA, Castanedes-Casey M, Dickson DW, Wszolek ZK, DCTN1 mutations in Perry syndrome, Nat. Genet, 41 (2009) 163–165. [PubMed: 19136952]

[42]. Puls I, Jonnakuty C, LaMonte BH, Holzbaur EL, Tokito M, Mann E, Floeter MK, Bidus K, Drayna D, Oh SJ, Brown RH Jr., Ludlow CL, Fischbeck KH, Mutant dynactin in motor neuron disease, Nat. Genet, 33 (2003) 455–456. [PubMed: 12627231]

[43]. Puls I, Oh SJ, Sumner CJ, Wallace KE, Floeter MK, Mann EA, Kennedy WR, Wendelschafer-Crabb G, Vortmeyer A, Powers R, Finnegan K, Holzbaur EL, Fischbeck KH, Ludlow CL, Distal

spinal and bulbar muscular atrophy caused by dynactin mutation, Ann. Neurol, 57 (2005) 687–694. [PubMed: 15852399]

[44]. Mishima T, Koga S, Lin WL, Kasanuki K, Castanedes-Casey M, Wszolek ZK, Oh SJ, Tsuboi Y, Dickson DW, Perry Syndrome: A Distinctive Type of TDP-43 Proteinopathy, J. Neuropathol. Exp. Neurol, 76 (2017) 676–682. [PubMed: 28789478]

[45]. Bignell GR, Warren W, Seal S, Takahashi M, Rapley E, Barfoot R, Green H, Brown C, Biggs PJ, Lakhani SR, Jones C, Hansen J, Blair E, Hofmann B, Siebert R, Turner G, Evans DG, Schrander-Stumpel C, Beemer FA, van Den Ouweland A, Halley D, Delpech B, Cleveland MG, Leigh I, Leisti J, Rasmussen S, Identification of the familial cylindromatosis tumour-suppressor gene, Nat. Genet, 25 (2000) 160–165. [PubMed: 10835629]

[46]. Hirokawa N, Noda Y, Tanaka Y, Niwa S, Kinesin superfamily motor proteins and intracellular transport, Nat Rev Mol Cell Biol, 10 (2009) 682–696. [PubMed: 19773780]

[47]. Lee H-J, Zheng JJ, PDZ domains and their binding partners: structure, specificity, and modification, Cell Communication and Signaling : CCS, 8 (2010) 8–8. [PubMed: 20509869]

[48]. Delevoye C, Miserey-Lenkei S, Montagnac G, Gilles-Marsens F, Paul-Gilloteaux P, Giordano F, Waharte F, Marks MS, Goud B, Raposo G, Recycling endosome tubule morphogenesis from sorting endosomes requires the kinesin motor KIF13A, Cell Rep, 6 (2014) 445–454. [PubMed: 24462287]

[49]. Delevoye C, Hurbain I, Tenza D, Sibarita JB, Uzan-Gafsou S, Ohno H, Geerts WJ, Verkleij AJ, Salamero J, Marks MS, Raposo G, AP-1 and KIF13A coordinate endosomal sorting and positioning during melanosome biogenesis, J. Cell Biol, 187 (2009) 247–264. [PubMed: 19841138]

[50]. Nakagawa T, Setou M, Seog D, Ogasawara K, Dohmae N, Takio K, Hirokawa N, A novel motor, KIF13A, transports mannose-6-phosphate receptor to plasma membrane through direct interaction with AP-1 complex, Cell, 103 (2000) 569–581. [PubMed: 11106728]

[51]. Zhou R, Niwa S, Guillaud L, Tong Y, Hirokawa N, A molecular motor, KIF13A, controls anxiety by transporting the serotonin type 1A receptor, Cell Rep, 3 (2013) 509–519. [PubMed: 23438369]

[52]. Najm J, Horn D, Wimplinger I, Golden JA, Chizhikov VV, Sudi J, Christian SL, Ullmann R, Kuechler A, Haas CA, Flubacher A, Charnas LR, Uyanik G, Frank U, Klopocki E, Dobyns WB, Kutsche K, Mutations of CASK cause an X-linked brain malformation phenotype with microcephaly and hypoplasia of the brainstem and cerebellum, Nat. Genet, 40 (2008) 1065–1067. [PubMed: 19165920]

[53]. Laverty HG, Wilson JB, Murine CASK is disrupted in a sex-linked cleft palate mouse mutant, Genomics, 53 (1998) 29–41. [PubMed: 9787075]

[54]. Lee S, Fan S, Makarova O, Straight S, Margolis B, A novel and conserved protein-protein interaction domain of mammalian Lin-2/CASK binds and recruits SAP97 to the lateral surface of epithelia, Mol. Cell. Biol, 22 (2002) 1778–1791. [PubMed: 11865057]

[55]. Roberts S, Delury C, Marsh E, The PDZ protein discs-large (DLG): the ‘Jekyll and Hyde’ of the epithelial polarity proteins, FEBS J, 279 (2012) 3549–3558. [PubMed: 22846345]

[56]. Iizuka-Kogo A, Shimomura A, Senda T, Colocalization of APC and DLG at the tips of cellular protrusions in cultured epithelial cells and its dependency on cytoskeletons, Histochem. Cell Biol, 123 (2005) 67–73. [PubMed: 15609045]

Highlights

1. The CAP-Gly domain-containing segment of kinesin motor KIF13B affects LRP1 functionality.
2. KIF13B forms a complex with LRP1 through the I_3 domain of hDLG1.
3. Deletion of mouse CAP-Gly domain region results in mislocalization of KIF13B and LRP1 resulting in serum cholesterol elevation.
4. Double mutations of KIF13A and KIF13B leads to perinatal lethality with developmental anomalies.

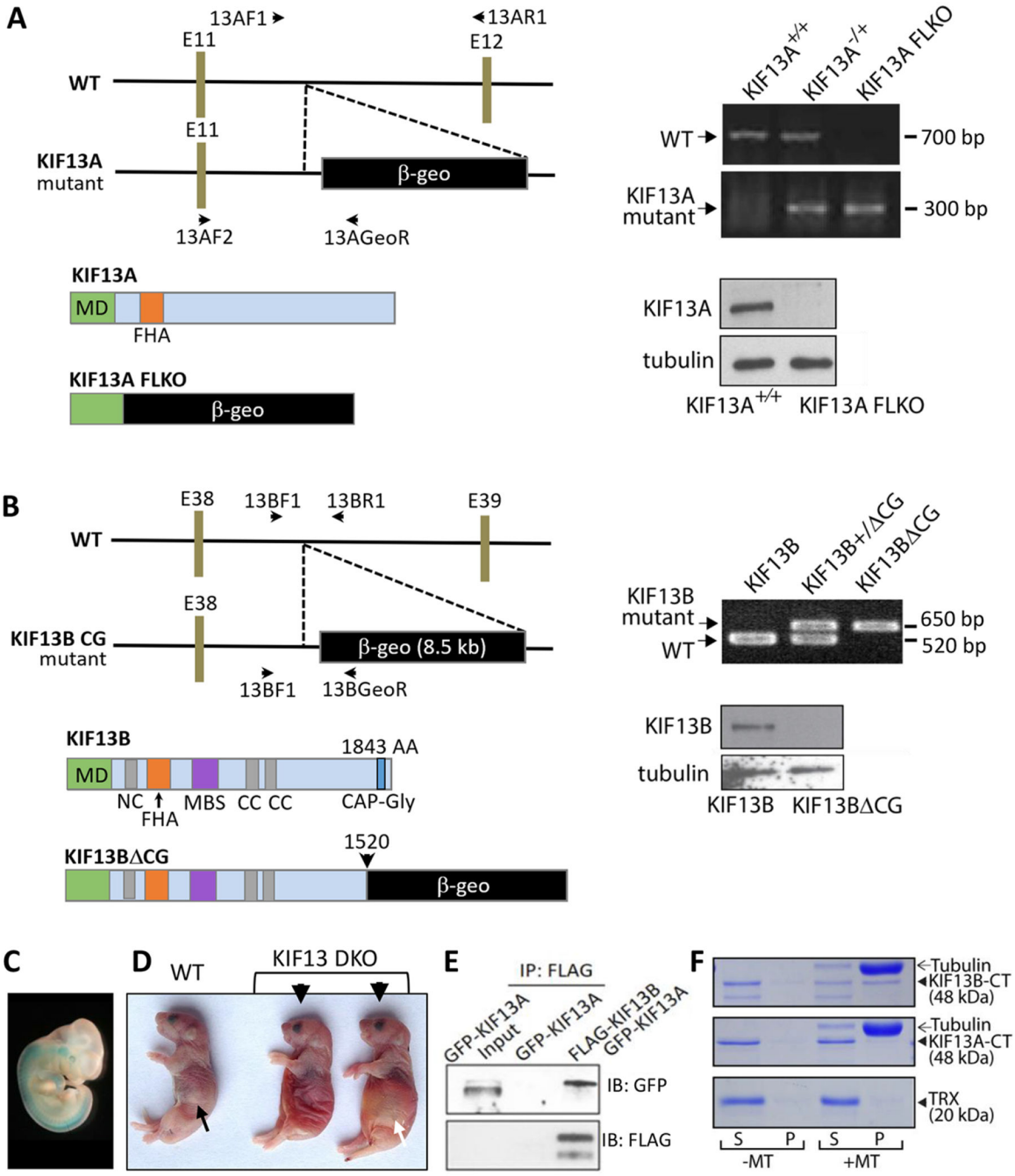

Fig. 1.

Generation of KIF13A knockout and KIF13B mutant mouse models. (A & B) Cartoons of KIF13A (A) and KIF13B (B) mouse models generated by β-geo cassette insertion and their verification by PCR (top right panel) and Western blotting (bottom right panel). (C) The LacZ staining showing expression of truncated KIF13B protein in KIF13BΔCG embryo E12.5. (D) A representative image of newborn WT and DKO (KIF13A and KIF13BΔCG) pups found dead shortly after birth. Arrowheads indicate face deformity (short snout). Black arrow indicates milk in the stomach whereas white arrow shows stomach full of air. (E) Co-

IP of GFP-KIF13A and FLAG-KIF13B co-transfected into FIEK293T cells. (F) Microtubule binding assay using the C-terminus of human KIF13B or human KIF13A tagged with TRX.

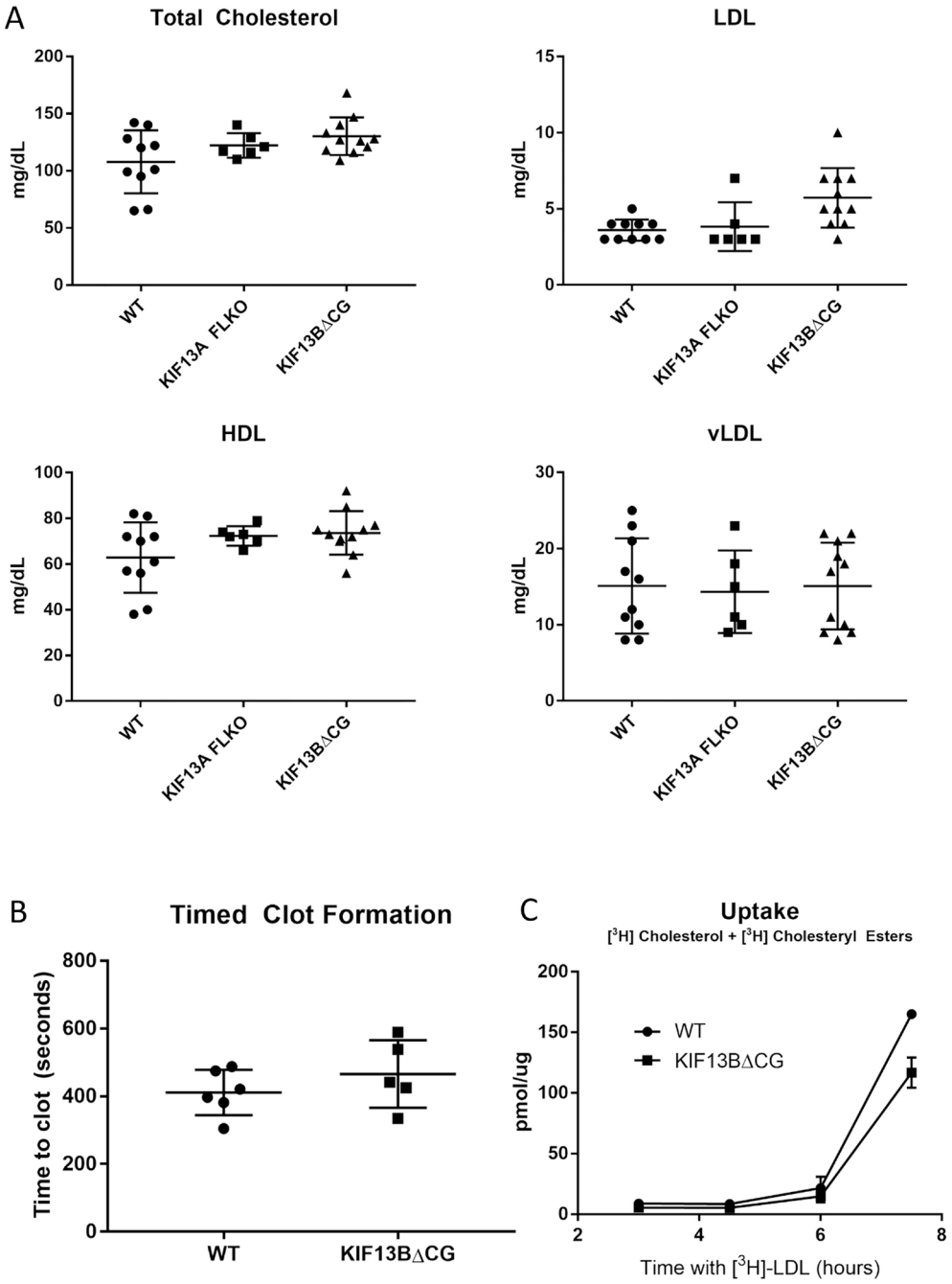

Fig. 2.

Characterization of lipid and factor VIII levels. (A) Lipid panel including total cholesterol, direct measurement of LDL, HDL, and VLDL of WT, KIF13A FLKO, and KIF13BΔCG serum from mice after 6 hours of fasting, n = 10 WT, 11 KIF13BΔCG, 6 KIF13A. Significant or nearly significant p values between WT and KIF13BΔCG: Total cholesterol, p = 0.033; LDL, p = 0.0042, HDL, p = 0.067. (B) Timed clot assay to measure factor VIII activity in WT and KIF13BΔCG mouse plasma, n = 5 for each genotype. (C) Time course of [^{3}H]CO-LDL uptake by MEFs from WT and KIF13BΔCG mice. MEFs were stimulated

with 50 ug/ml of [^{3}H]CO-LDL for 3, 4.5, 6, and 7.5 hours, and the amount of [^{3}H]CO taken into the cells was measured. Measurements are from triplicate wells.

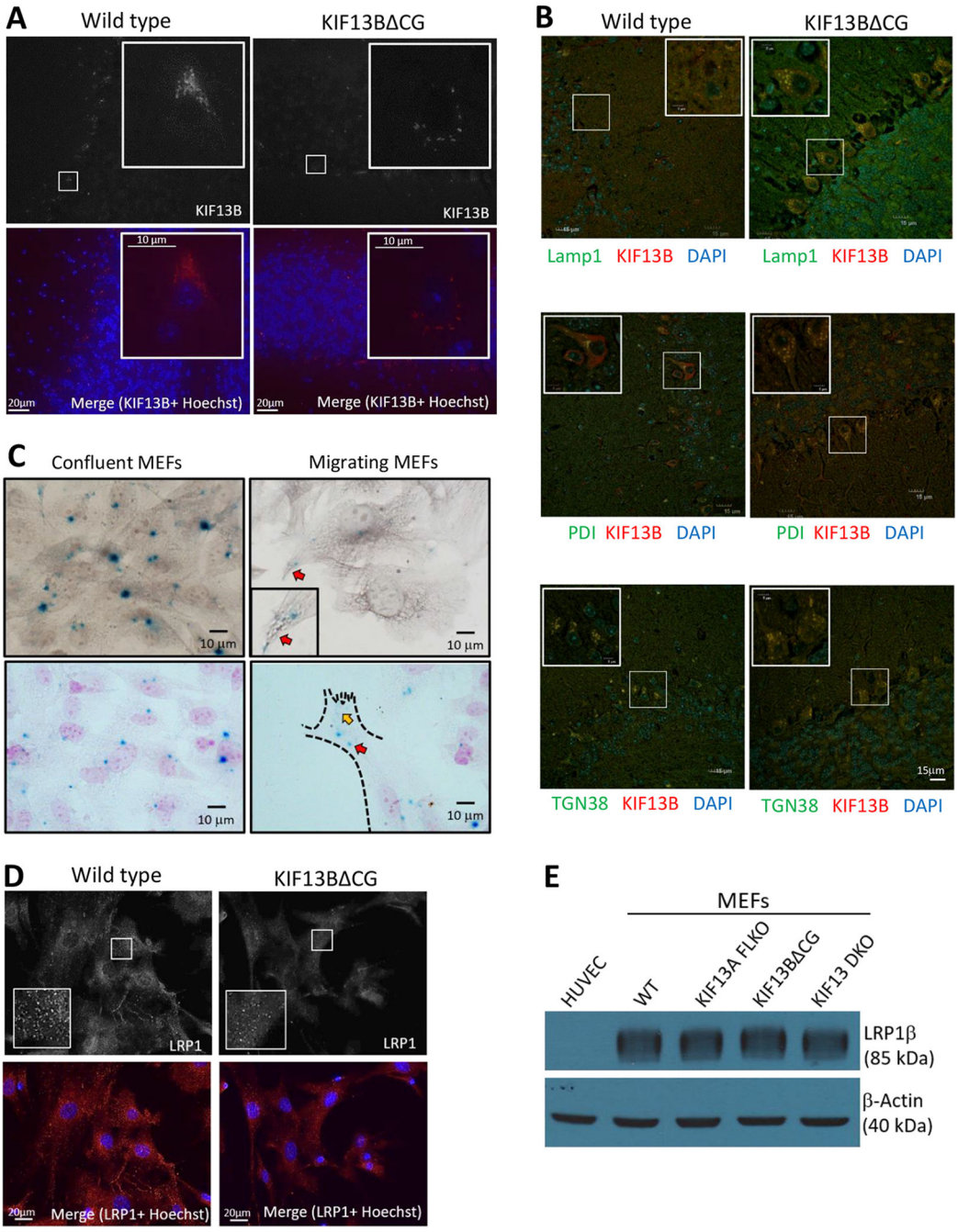

Fig. 3.

Subcellular localization of KIF13B and LRP1. (A, B, C) Localization of KIF13B in brain tissue from WT or KIF13BΔCG mice. (A & B) Paraffin-embedded sections of brain were stained with a polyclonal Ab that recognizes the N-terminus of KIF13B (red), which is present in both WT and KIF13BΔCG proteins, and nuclear counterstain with Hoechst or DAPI (blue) (A) and double stained with organelle specific markers (green) LAMP1 (B, top), PDI (B, middle), or TGN38 (B, bottom). Images were taken at 400X (A) or 600X (B), and insets are magnifications of up to two cells. Each image is a representativetion of

truncated KIF13B in confluent culture of MEFs (left) and after the scratch wound in MEFs to initiate cell migration (right). KIF13BΔCG can migrate to the leading edge of the fibroblasts (red arrows). Top panels were co-stained with β-tubulin and bottom panels show counter staining with Nuclear Fast Red. Of note, we performed γ-tubulin staining in fibroblasts to detect the position of MTOC. However, the double staining of γ-tubulin and LacZ activity was not feasible because the blue signal from LacZ stain completely masks the faint signal from the γ-tubulin (data reviewed but not shown). The blue dots appear to be reminiscent of the MTOC. (D) LRP1 subcellular localization in MEFs from WT or KIF13BΔCG mice. MEFs were stained with LRP1 (red) and nuclear counterstain with Hoechst (blue). Images were taken at 400X and a representative frame from three independent observations is shown. (E) LRP1 steady state protein expression in MEFs detected by Western blotting. Lysate from HUVECs served as a negative control for the LRP1 expression, and β-actin was used as a loading control.

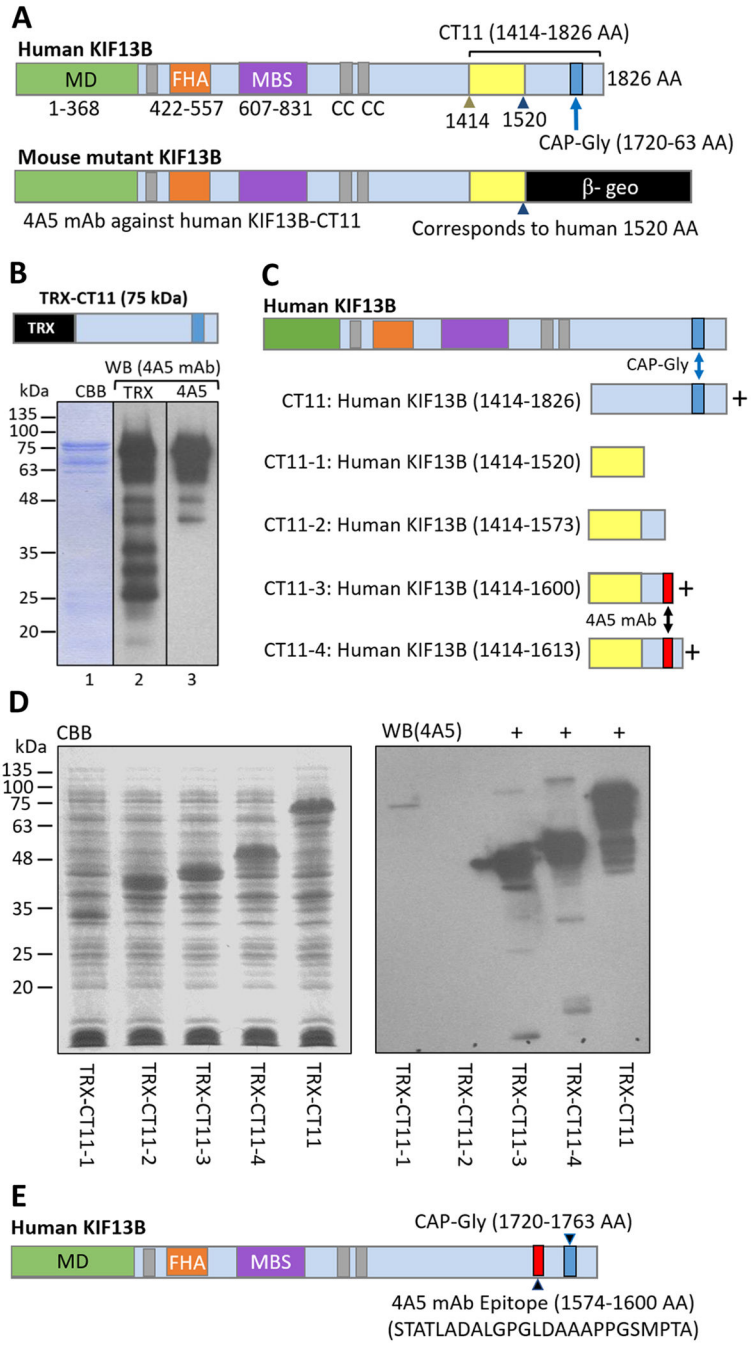

Fig. 4.

Localization of 4A5 monoclonal antibody epitope in KIF13B. (A) Schematic representation of human KIF13B and mouse mutant KIF13BΔCG. Mouse mutant KIF13B truncates at the position corresponding to 1520 AA in the human sequence. (B) Western blot analysis of TRX-CT11. Purified recombinant TRX-CT11 protein was detected by Coomassie Brilliant Blue (CBB) stain (lane 1), and Western blotting with anti-TRX mAb (lane 2) and anti-KIF13B mAb 4A5 (lane 3). (C) Recombinant protein constructs of KIF13B used to map the epitope of 4A5 mAb by Western blotting. (D) Total cell lysates of bacterially expressed

proteins were analyzed by CBB stain (left panel) and Western blotting with 4A5 mAb (right panel). (E) Position of the 4A5 mAb epitope relative to the CAP-Gly domain within human KIF13B sequence. The 4A5 mAb epitope is deleted in KIF13BΔCG.

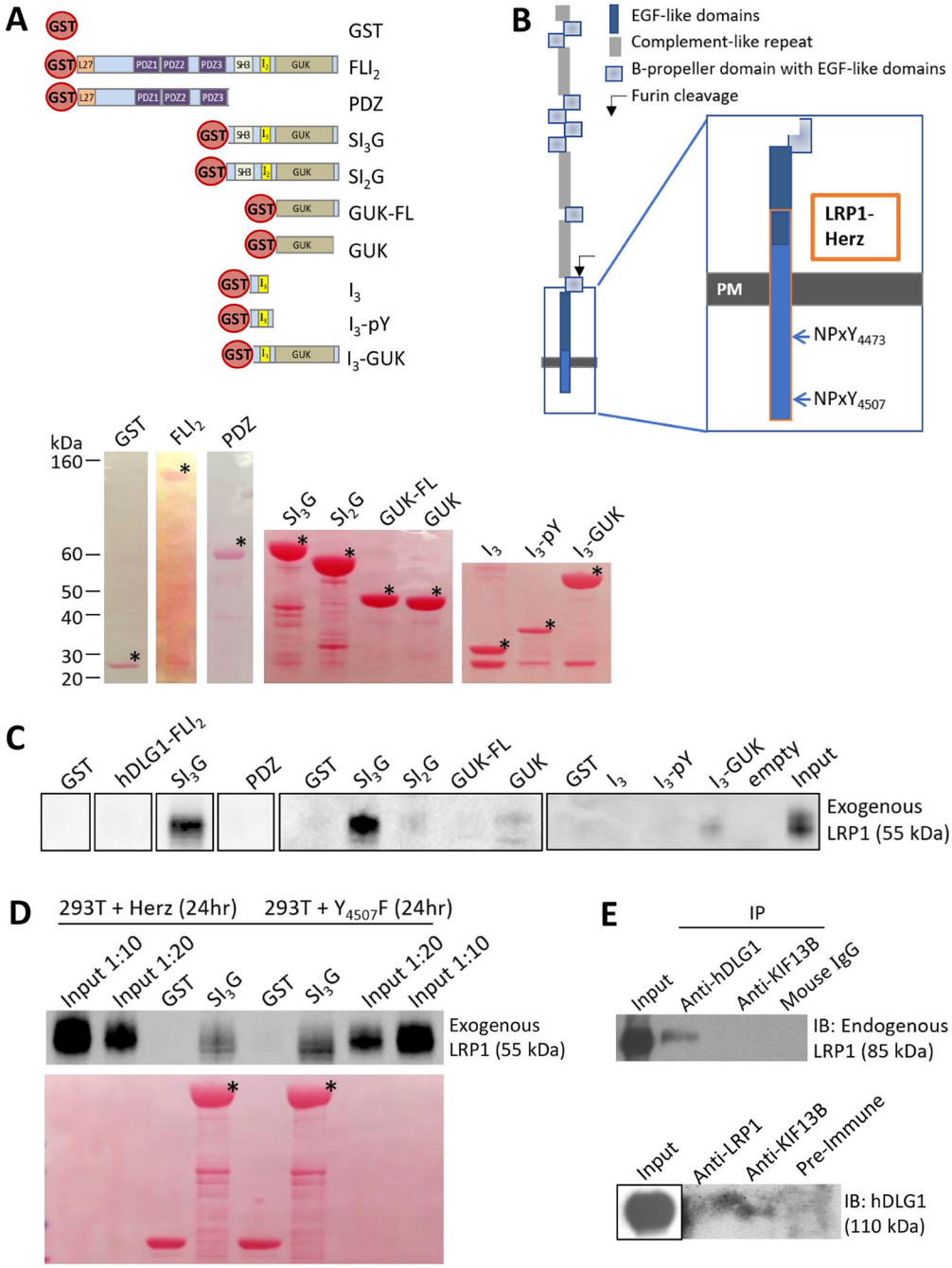

Fig. 5.

Identification of I_3 domain of hDLG1 as the binding site for LRP1. (A) Schematics of multiple GST-hDLG1 constructs used in the pull-down assays. Ponceau staining (below) shows expression of each GST fusion protein marked by an*. GST= tag only, FLI_2= full length hDLG1 with insert 2, PDZ = PDZ domains 1,2, and 3, SI_3G=SH3-insert 3-GUK domains, SI_2G=SH3-insert 2-GUK domains, GUK=GUK domain, GUK-FL=GUK domain and C-terminus, I_3=insert 3 only, I_3-pY=I_3 insert with pY segment, I_3-GUK= Insert 3-GUK domains. All constructs contained the N-terminal GST tag. (B) Cartoon of LRP1 focusing

on the LRPI-β segment to identify the boundary of LRP1-Herz construct and location of NPxY motifs. The LRP1-Y4507 is mutated to LRP1-Y4507F. PM = plasma membrane. (C) Immunoblotting of LRP1-Herz in pull down assays from transfected FIEK293T cell lysates. LRP1 antibody detected exogenous LRPI-β (65 kDa) in the input lane, and in lanes corresponding to the beads that contained the I_3 domain of hDLG1. (D) Immunoblotting of LRP1-Herz or LRP1-Y4507F in the pull-down assays from transfected HEK293T cell lysates. LRP1 mAb detected exogenous LRPI-β (65 kDa) in the input lane, and in lanes corresponding to the beads that contained the I_3 domain of DLG1. Ponceau staining verified even loading and expression of GST constructs marked by an*. (E) Co-IP of LRP1 using an anti-hDLG1 mAb, anti-KIF13B mAb, and mouse IgG as negative control in the membrane fraction of HepG2 cells (top). Co-IP of DLG1 using an anti-LRP1 mAb, anti-KIF13B mAb, and pre-immune rabbit serum as negative control. The input lane is from the same membrane, but a shorter exposure is presented.

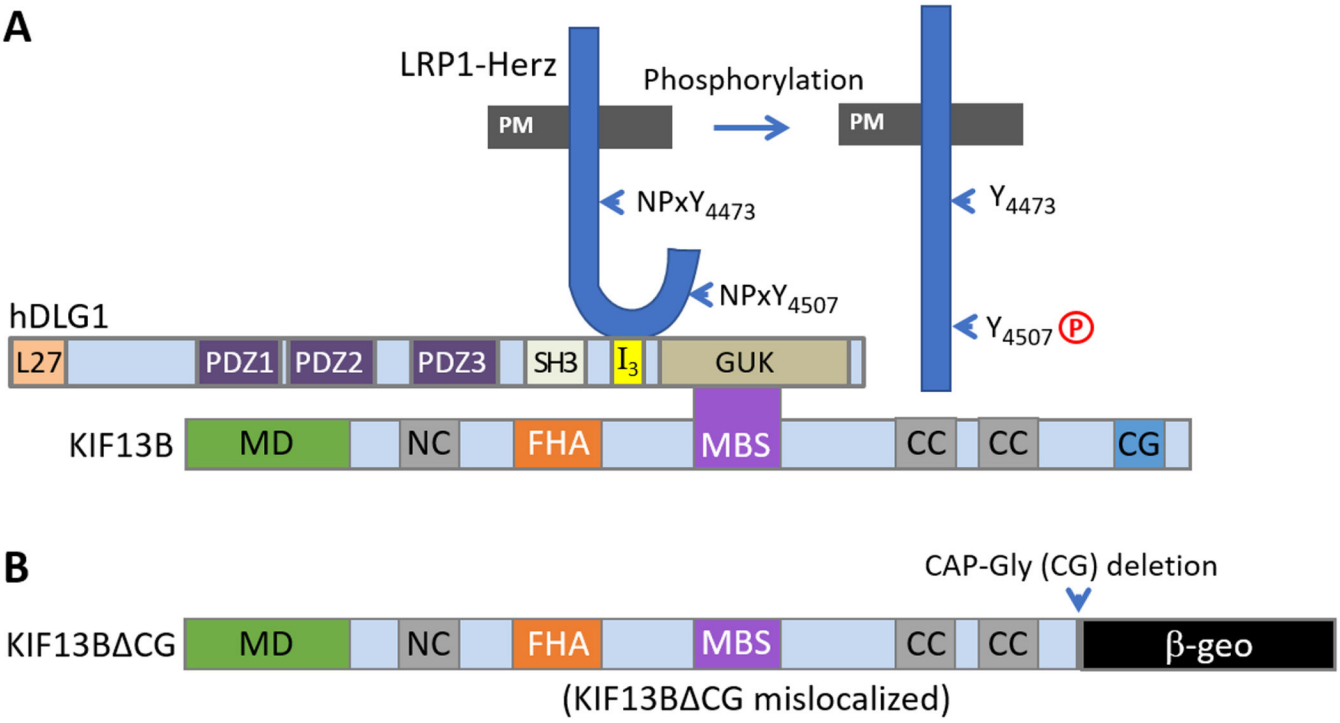

Fig. 6.

A proposed model for the LRP1-DLG1-KIF13B complex formation. (A) DLG1 serves as an adaptor by linking LRP1 with KIF13B. The LRP1-CT binds to the I_3 domain of DLG1, which in turn utilizes its GUK domain to bind to the MBS domain of KIF13B. This model predicts that phosphorylation of Y4507 of LRP1-CT may induce a conformational change in its cytoplasmic domain that regulates its binding to DLG1. (B) A cartoon of truncated KIF13B expressed in KIF13BΔCG mice. The truncated KIF13B is mislocalized or destabilized at the plasma membrane preventing its interaction with DLG1 and suppressing LRP1 endocytosis.